

Interactions between Intracellular Domains as Key Determinants of the Quaternary Structure and Function of Receptor Heteromers*[§]

Received for publication, February 18, 2010, and in revised form, June 7, 2010. Published, JBC Papers in Press, June 18, 2010, DOI 10.1074/jbc.M110.115634

Gemma Navarro[‡], Sergi Ferré[§], Arnau Cordomi[¶], Estefania Moreno[‡], Josefa Mallol[‡], Vicent Casadó[‡], Antoni Cortés[‡], Hanne Hoffmann^{||}, Jordi Ortiz^{||}, Enric I. Canela[‡], Carme Lluís[‡], Leonardo Pardo[¶], Rafael Franco^{***}, and Amina S. Woods^{§1}

From the [‡]Centro de Investigación Biomédica en Red Sobre Enfermedades Neurodegenerativas, Department of Biochemistry and Molecular Biology, Faculty of Biology, University of Barcelona, 08028 Barcelona, Spain, the [§]Intramural Research Program, National Institute on Drug Abuse, Department of Health and Human Services, Baltimore, Maryland 21224, the [¶]Laboratori de Medicina Computacional, Unitat de Bioestadística, and ^{||}Neuroscience Institute and Department of Biochemistry and Molecular Biology, Facultat de Medicina, Universitat Autònoma de Barcelona, 08193 Bellaterra, Spain, and the ^{***}Centro de Investigación Médica Aplicada, Universidad de Navarra, 31008 Pamplona, Spain

G protein-coupled receptor (GPCR) heteromers are macromolecular complexes with unique functional properties different from those of its individual protomers. Little is known about what determines the quaternary structure of GPCR heteromers resulting in their unique functional properties. In this study, using resonance energy transfer techniques in experiments with mutated receptors, we provide for the first time clear evidence for a key role of intracellular domains in the determination of the quaternary structure of GPCR heteromers between adenosine A_{2A}, cannabinoid CB₁, and dopamine D₂ receptors. In these interactions, arginine-rich epitopes form salt bridges with phosphorylated serine or threonine residues from CK1/2 consensus sites. Each receptor (A_{2A}, CB₁, and D₂) was found to include two evolutionarily conserved intracellular domains to establish selective electrostatic interactions with intracellular domains of the other two receptors, indicating that these particular electrostatic interactions constitute a general mechanism for receptor heteromerization. Mutation experiments indicated that the interactions of the intracellular domains of the CB₁ receptor with A_{2A} and D₂ receptors are fundamental for the correct formation of the quaternary structure needed for the function (MAPK signaling) of the A_{2A}-CB₁-D₂ receptor heteromers. Analysis of MAPK signaling in striatal slices of CB₁ receptor KO mice and wild-type littermates supported the existence of A₁-CB₁-D₂ receptor heteromer in the brain. These findings allowed us to propose the first molecular model of the quaternary structure of a receptor heteromultimer.

Receptor heteromers are the focus of intense research, as through heteromerization receptors become unique functional entities with different properties from those of either receptor when not engaged in heteromerization resulting in new therapeutic targets (1–4). Their unique properties provide a “biochemical fingerprint” thus allowing their identification in native tissues (1, 3). There is already a long list of discovered heteromers with two different G protein-coupled receptors (GPCRs)² (2, 4). Furthermore, we recently obtained evidence for the existence of receptor heteromultimers, *i.e.* heteromers including more than two different receptors, and reported on heteromers, including the GPCRs adenosine A_{2A}, cannabinoid CB₁, and dopamine D₂ receptors, in transfected cells (5). Evidence of GPCR homomultimers has also been recently demonstrated in living cells (6, 7). Many important questions regarding receptor heteromers and heteromultimers remain unanswered. What is the arrangement of their GPCR units (quaternary structure)? What are the molecular determinants of their quaternary structure? Last but not least, what is their functional significance in native tissues?

It was inferred that different molecular mechanisms were involved in GPCR homo- and heteromerization. For family C GPCRs, disulfide bonds between extracellular domains as well as coiled-coil interactions between C-terminal domains seem to be necessary for the formation of functional homomeric or heteromeric receptors (8). For oligomerization of family A GPCRs, the helical transmembrane (TM) domains seem to be particularly important (7, 9–15). In this study, by using mutated A_{2A}, CB₁, and D₂ receptors, we investigated the relevance of electrostatic interactions (16) between intracellular domains in the determination of the quaternary structure of GPCR heteromers between A_{2A}, CB₁, and D₂ receptors. Our initial goal was to obtain evidence for multiple intracellular interactions in the A_{2A}-CB₁-D₂ receptor heteromultimer. Significantly, the same intracellular domains involved in A_{2A}-CB₁-D₂ receptor heteromultimerization were also involved in

* This work was supported, in whole or in part, by a National Institutes of Health grant from intramural funds to NIDA. This work was also supported by Spanish Ministerio de Ciencia y Tecnología Grants SAF2008-00146, SAF2006-05481, and SAF2008-03229-E/ for ERA-NET Coordination of Research Activities and Instituto de Salud Carlos III (RD07/0067/0008) Grant 060110 from Fundació La Marató de TV3.

[§] The on-line version of this article (available at <http://www.jbc.org>) contains supplemental Figs. 1 and 2 and Table 1.

¹ To whom correspondence should be addressed: National Institute on Drug Abuse, Intramural Research Program, Department of Health and Human Services, 333 Cassell Dr., Baltimore, MD 21224. Tel.: 443-740-2747; Fax: 443-740-2144; E-mail: awoods@intra.nida.nih.gov.

² The abbreviations used are: GPCR, G protein-coupled receptor; SRET, sequential resonance energy transfer; ANOVA, analysis of variance; PDB, Protein Data Bank; BRET, bioluminescence resonance energy transfer; TM, transmembrane; IL3, intracellular loop 3.

A_{2A} - D_2 , A_{2A} - CB_1 , and CB_1 - D_2 receptor heteromerization. A three-dimensional model of the quaternary structure of the receptor heteromultimer was obtained by using the information from resonance energy transfer between A_{2A} , CB_1 , and D_2 receptors in the receptor heteromultimer. Furthermore, a biochemical property of the receptor heteromultimer was found to be dependent on its correct quaternary structure, determined by the intracellular electrostatic interactions, which allowed its identification in rodent brain tissue.

EXPERIMENTAL PROCEDURES

Cell Culture—HEK-293T cells were grown in Dulbecco's modified Eagle's medium (DMEM) (Invitrogen) supplemented with 2 mM L-glutamine, 100 units/ml penicillin/streptomycin, and 5% (v/v) heat-inactivated fetal bovine serum (FBS) (all supplements were from Invitrogen). CHO cell lines were maintained in α -minimal essential medium without nucleosides, containing 10% fetal calf serum, 50 μ g/ml penicillin, 50 μ g/ml streptomycin, and 2 mM L-glutamine (300 μ g/ml). Cells were maintained at 37 °C in an atmosphere of 5% CO_2 and were passaged when they were 80–90% confluent, twice a week.

Mutant Receptors—Ser³⁷⁴ in the C-terminal domain of the human A_{2A} receptor was mutated to Ala to obtain the A_{2A} ^{A374} receptor. The sequence ¹⁹⁹RIFLAARRQ²⁰⁷ (boldface letters indicate the amino acid involved in the interaction between the receptors and the residues that were mutated) in the cytoplasm at the end of TM5 of human A_{2A} receptor was mutated to ¹⁹⁹RIFLAAAQ²⁰⁷ to obtain the A_{2A} ^{A205-A206} receptor. The sequence ⁴⁶²SVSTDTSAE⁴⁷⁰ in the C-terminal domain of human CB_1 receptor was mutated to ⁴⁶²SVSTDAAAE⁴⁷⁰ to obtain the CB_1 ^{A467-A468} receptor. The sequence ³²¹TSEDGKQVT³³⁰ in the third intracellular loop of human CB_1 receptor was mutated to ³²¹AAEDGKQVT³³⁰ to obtain CB_1 ^{A321-A322} receptor. Mutations were performed by site-directed mutagenesis (Cellogenetics, Ijamsville, MD).

Fusion Proteins and Expression Vectors—The human cDNAs of the A_{2A} , CB_1 , and the mutant versions of these receptors or the human D_2 , D_{2S} , and $D_{4.4}$ receptors, cloned in *pcDNA3.1*, were amplified without their stop codons using sense and antisense primers harboring unique EcoRI and BamHI sites to clone A_{2A} , A_{2A} ^{A374}, and A_{2A} ^{A205-A206} receptors in the *Rluc* corresponding vector, EcoRI and KpnI to clone D_2 and D_{2S} receptors in the GFP² corresponding vector, BamHI and EcoRI to clone CB_1 , CB_1 ^{A467-A468}, and CB_1 ^{A321-A322} in the enhanced YFP corresponding vector, and XhoI and BamHI sites to clone $D_{4.4}$ receptor in the *Rluc* corresponding vector. The amplified fragments were subcloned to be in-frame into restriction sites of the multiple cloning sites of *pcDNA3.1-Rluc*, *pGFP²-N3(h)*, *pEYFP-N1* (Clontech) to give the plasmids corresponding to A_{2A} -*Rluc*, A_{2A} ^{A374}-*Rluc*, A_{2A} ^{A205-A206}-*Rluc*, D_4 -*Rluc*, D_2 -GFP², D_{2S} -GFP², CB_1 -YFP, CB_1 ^{A467-A468}-YFP, and CB_1 ^{A321-A322}-YFP receptor fusion proteins. The cDNA of the 5HT_{2B}-YFP fusion protein was kindly provided by Dr. Irma Nardi (University of Pisa, Italy). Under these conditions, the fusion proteins are expressed at the membrane level, are not strongly overexpressed, and are quantitatively expressed in similar amounts (5).

Transient Transfection and Sample Preparation—HEK-293T or CHO cells growing in 6-well dishes were transiently transfected with the corresponding fusion protein cDNA by the polyethyleneimine method (Sigma). Cells were incubated (4 h) with the corresponding cDNA together with polyethyleneimine (5.47 mM in nitrogen residues) and 150 mM NaCl in a serum-starved medium. After 4 h, the medium was changed to a fresh complete culture medium. Forty eight hours after transfection, cells were washed twice in quick succession in Hanks' balanced salt solution with 10 mM glucose, detached, and resuspended in the same buffer containing 1 mM EDTA. To control the cell number, sample protein concentration was determined using a Bradford assay kit (Bio-Rad) using bovine serum albumin dilutions as standards. Cell suspension (20 μ g of protein) was distributed into 96-well microplates; black plates with transparent bottom were used for FRET and fluorescence determinations, and white plates with white bottom were used for BRET and SRET experiments.

BRET Experiments—HEK-293T cells expressing the corresponding donor (receptor *Rluc*) and increasing amounts of the corresponding acceptor (receptor GFP² for BRET² or receptor YFP for BRET¹), as indicated in figure legends, were used. With aliquots of transfected cells (20 μ g of protein), three different determinations were performed in parallel. (i) To quantify fluorescence proteins expression, cells were distributed in 96-well microplates (black plates with transparent bottom), and fluorescence was read in a Fluostar Optima Fluorimeter (BMG Labtechnologies, Offenburg, Germany) equipped with a high energy xenon flash lamp, using an excitation filter at 410 nm for receptor GFP² reading (BRET²) or 485 nm for receptor YFP reading (BRET¹), and emission was detected using filters at 510 nm (for GFP²) or 530 nm (for YFP). Receptor fluorescence expression was determined as fluorescence of the sample minus the fluorescence of cells expressing receptor *Rluc* alone. (ii) For BRET² and BRET¹ measurements, the equivalent of 20 μ g of cell suspension was distributed in 96-well microplates (Corning 3600, white plates with white bottom), and 5 μ M DeepBlueC (BRET²) or coelenterazine H (BRET¹) (Molecular Probes, Eugene, OR) was added. For BRET² experiments, readings were collected immediately (~30 s) after addition of DeepBlueC using a Mithras LB 940 (Berthold Technologies, DLReady, Germany) that allows the integration of the signals detected in the short wavelength filter at 410 nm and the long wavelength filter at 510 nm. In BRET¹ after 1 min of adding coelenterazine H, the readings were collected using a Mithras LB 940 that allows the integration of the signals detected in the short wavelength filter at 485 nm and the long wavelength filter at 530 nm. (iii) To quantify receptor *Rluc* expression, luminescence readings were performed after 10 min of adding 5 μ M coelenterazine H. The net BRET is defined as ((long wavelength emission)/(short wavelength emission)) – *Cf*, where *Cf* corresponds to ((long wavelength emission)/(short wavelength emission)) for the *Rluc* construct expressed alone in the same experiment.

FRET Experiments—HEK-293T cells expressing the corresponding donor (receptor GFP²) and increasing amounts of the corresponding acceptor (receptor YFP), as indicated in figure legends, were used. Using aliquots of transfected cells (20 μ g of protein), two different determinations were performed in par-

Quaternary Structure of Receptor Heteromers

allel. (i) To quantify YFP fluorescence, due to receptor YFP expression, the same procedure as described for BRET experiments was used. (ii) For FRET measurements, the equivalent of 20 μg of cell suspension was distributed into 96-well microplates (black plates with a transparent bottom) and read in a Fluostar Optima fluorimeter equipped with a high energy xenon flash lamp, using an excitation filter at 410 nm and an emission filters at 510 nm (Ch_x) and 530 nm (Ch_y). Gain settings were identical for all experiments to keep the relative contribution of the fluorophores to the detection channels constant for spectral unmixing. The contribution of GFP² and YFP proteins alone to the two detection channels (spectral signature (17)) was measured in experiments with cells expressing only one of these proteins and normalized to the sum of the signal obtained in the two detection channels. The spectral signatures of the different receptors fused to either GFP² or YFP did not vary significantly from the determined spectral signatures of the fluorescent proteins alone. In determinations i and ii, linear unmixing was done taking into account the spectral signature as described by Zimmermann *et al.* (17) to separate the two emission spectra. For quantitation of the fluorescence emitted by each of two individual fluorophores (FluoA corresponding to the donor and FluoB corresponding to the acceptor) in FRET experiments, Equation 1 was applied,

$$\begin{aligned}\text{FluoA} &= S/(1 + 1/R) \\ \text{FluoB} &= S/(1 + R) \\ \text{Being} & \hspace{15em} (\text{Eq. 1}) \\ S &= \text{Ch}_x + \text{Ch}_y \\ R &= (B_y Q - B_x)/(A_x - A_y Q) \\ Q &= \text{Ch}_x/\text{Ch}_y\end{aligned}$$

where Ch_x and Ch_y represent the signals in detection channels x and y , and A_x , B_x and A_y , B_y represent the normalized contributions of FluoA or FluoB to channels x and y , as they are known from the spectral signatures of the fluorescent proteins.

Sequential Resonance Energy Transfer (SRET) Experiments—The recently introduced sequential BRET-FRET (SRET) technique (5) not only allows the demonstration of heteromerization of three proteins but can also provide information about the quaternary structure of the heterotrimeric complex. By transfecting three receptors separately fused to *Rluc*, GFP², and YFP, the detection of the SRET² signal demonstrates the physical interactions between the three receptors. In SRET², the oxidation of the *Rluc* substrate DeepBlueC triggers GFP² excitation (BRET²), which triggers a subsequent excitation of YFP (FRET) (see Fig. 1). Emission of YFP after addition of DeepBlueC is only possible if the three fusion proteins are in close proximity (<10 nm), allowing bioluminescent and fluorescent SRET to occur. For SRET experiments, HEK-293T cells were transiently co-transfected with the indicated amounts of plasmid cDNAs corresponding to receptor *Rluc*, receptor GFP², and receptor YFP (see figure legends). In the experiments without casein kinase 1/2 inhibitors, cells were used 48 h post-transfection. When using casein kinase 1/2 inhibitors, cells were treated with casein kinase I inhibitor IC 261 (50 μM ; Cal-

biochem) and casein kinase 2 inhibitor TBAC (10 μM ; Calbiochem) 4 h after transfection, and after 24 h, the medium was changed to a fresh complete culture medium containing the same amount of inhibitors, and cells were used 48 h post-transfection. Using aliquots of transfected cells (20 μg of protein), different determinations were performed in parallel. (i) Quantification of protein-YFP expression was performed as indicated in FRET experiments. The sample fluorescence is the fluorescence calculated as described minus the fluorescence of cells expressing only protein-*Rluc* and protein-GFP². (ii) Quantification of protein-*Rluc* expression was by determination of the luminescence due to protein-*Rluc*. Cells were distributed in 96-well microplates (Corning 3600, white plates with white bottom), and luminescence was determined 10 min after addition of 5 μM coelenterazine H in a Mithras LB 940 multimode reader. (iii) BRET and FRET were combined to generate a technique called sequential BRET-FRET (SRET) that permits identification of heteromers formed by three different proteins. Cells were distributed in 96-well microplates (Corning 3600, white plates with white bottom), and 5 μM DeepBlueC (Molecular Probes, Eugene, OR) was added. The SRET² signal was collected using a Mithras LB 940 reader with detection filters for short wavelength (410 nm) and long wavelength (530 nm). By analogy with BRET, net SRET² is defined as ((long wavelength emission)/(short wavelength emission)) - C_f , where C_f corresponds to long wavelength emission/short wavelength emission for cells expressing protein-*Rluc* and protein-GFP². Linear unmixing was done for SRET² quantification, taking into account the spectral signature to separate the two fluorescence emission spectra (17). (iv) Using aliquots of cells transfected for SRET experiments, BRET¹, BRET², and FRET measurements were performed as indicated above. A SRET² saturation curve can be obtained determining SRET² as a function of increasing expression of the FRET acceptor (receptor YFP). From these saturation curves, an apparent SRET_{max} was determined by fitting data to a monophasic saturation curve by nonlinear regression using the commercial Graftit curve-fitting software (Erithacus Software, Surrey, UK). These parameters have a similar meaning to these parameters when applied to BRET assays (5).

ERK Phosphorylation Assays—Wild-type littermates and CB₁ receptor knock-out CD1 albino Swiss male mice, 8 weeks old, weighing 25 g were used. The generation of mice lacking CB₁ receptor has been described elsewhere (18, 19). Mice were housed five per cage in a temperature- (21 \pm 1 $^\circ\text{C}$) and humidity-controlled (55 \pm 10%) room with a 12:12 h light/dark cycle (light between 08:00 and 20:00 h) with food and water *ad libitum*. Animal procedures were conducted according to standard ethical guidelines (European Communities Council Directive 86/609/EEC) and approved by the Local Ethical Committee (IMAS-IMIM/UPF). Mice were decapitated with a guillotine, and the brains were rapidly removed and placed in ice-cold oxygenated (O_2/CO_2 , 95:5%) Krebs-HCO₃⁻ buffer (124 mM NaCl, 4 mM KCl, 1.25 mM NaH₂PO₄, 1.5 mM MgCl₂, 1.5 mM CaCl₂, 10 mM glucose, and 26 mM NaHCO₃, pH 7.4). The brains were sliced at 4 $^\circ\text{C}$ in a brain matrix (Zivic Instruments, Pittsburgh, PA) into 0.5-mm coronal slices. Slices were kept at 4 $^\circ\text{C}$ in Krebs-HCO₃⁻ buffer during the dissection of the striatum.

Each slice was transferred into an incubation tube containing 1 ml of ice-cold Krebs-HCO₃⁻ buffer. The temperature was raised to 23 °C, and after 30 min, the media were replaced by 2 ml of Krebs-HCO₃⁻ buffer (23 °C). The slices were incubated under constant oxygenation (O₂/CO₂, 95:5%) at 30 °C for 4–5 h in an Eppendorf thermomixer (Eppendorf-5 Prime, Inc., Boulder, CO). The media were replaced by 200 μl of fresh Krebs-HCO₃⁻ buffer, and after 30 min, 1 μM of the A_{2A} receptor agonist CGS-21680, 1 μM of the D₂ receptor agonist quinpirole, or both prepared in Krebs-HCO₃⁻ buffer were added. After 10 min, the incubation solution was discarded, and slices were frozen on dry ice and stored at -80 °C. When ERK phosphorylation assays were performed in cell cultures, CHO cells (48 h after transfection) were cultured in serum-free medium for 16 h before the addition of any agent. Cells were resuspended in Hanks' balanced salt solution buffer and were treated for 5 min with CGS2168 (200 nM), quinpirole (1 μM), or a mixture of both ligands and rinsed with ice-cold phosphate-buffered saline. Both cells and slices were lysed by the addition of 500 μl of ice-cold lysis buffer (50 mM Tris-HCl, pH 7.4, 50 mM NaF, 150 mM NaCl, 45 mM β-glycerophosphate, 1% Triton X-100, 20 μM phenylarsine oxide, 0.4 mM NaVO₄, and protease inhibitor mixture). The cellular debris was removed by centrifugation at 13,000 × g for 5 min at 4 °C, and the protein was quantified by the bicinchoninic acid method using bovine serum albumin dilutions as standard. To determine the level of ERK1/2 phosphorylation, equivalent amounts of protein (10 μg) were separated by electrophoresis on a denaturing 7.5% SDS-polyacrylamide gel and transferred onto PVDF membranes. The membranes were then probed with a mouse anti-phospho-ERK1/2 antibody (Sigma, 1:2500). To rule out that the differences observed were due to the application of unequal amounts of lysates, PVDF blots were stripped and probed with a rabbit anti-ERK1/2 antibody that recognizes both phosphorylated and nonphosphorylated ERK1/2 (Sigma, 1:40,000). Bands were visualized by the addition of anti-mouse HRP-conjugated (Dako, Glostrup, Denmark) or anti-rabbit HRP-conjugated (Sigma) secondary antibodies, respectively, and SuperSignal West Pico chemiluminescent substrate (Pierce). Bands densities were quantified with LAS-3000 (Fujifilm), and the level of phosphorylated ERK1/2 isoforms was normalized for differences in loading using the total ERK protein band intensities. Quantitative analysis of detected bands was performed by Image Gauge version 4.0 software. Bifactorial ANOVA and post hoc Bonferroni tests were used for statistical comparisons.

Mass Spectrometric Analysis—0.3 μl of equimolar solutions of the various peptides were deposited on the sample plate followed by 0.3 μl of matrix, a saturated solution of 2,4,6-trihydroxyacetophenone in 50% ethanol, and left to dry at room temperature. Spectra of each sample spot were acquired using a MALDI TOF-TOF instrument (Applied Biosystem 4700 proteomics analyzer, Framingham, MA) in positive ion mode. Each spectrum is the average of 1000 shots. All peptides were synthesized at The Johns Hopkins School of Medicine "Synthesis and Sequencing Facility."

Computational Models of D₂, CB₁, and A_{2A} Receptors—The amino acid sequences of the human D₂ receptor (accession number P14416), CB₁ receptor (P21554), and A_{2A} receptor

(P29274) receptors were obtained from UniProt. Structural simulations of the A_{2A} receptor are based on its crystal structure (PDB code 3EML) (20). Simulations of the D₂ and CB₁ receptors are based on computational models constructed by homology modeling techniques using the crystal structure of the β₂-adrenergic receptor (PDB code 2RH1) (21, 22) as template. Because of the absence of P5.50 Ballesteros-Weinstein numbering (23) in the CB₁ receptor, we superimposed Tyr²⁹²(5.58) and Lys³⁰⁰(5.66) to Tyr²¹⁹(5.58) and Lys²²⁷(5.66) of the β₂-adrenergic receptor. Tyr5.58 and Lys5.66 are structural and functional amino acids involved in the stabilization of the active state by interacting with Arg3.50 and Asp/Glu6.30, respectively, as revealed by the recent crystal structure of the ligand-free opsin, which contains several distinctive features of the active state (24). The highly conserved NPXXYX_{n=5,6}F(K/R) motif at the junction between TM7 and Hx8 is one residue shorter in the β₂-adrenergic receptor (n = 5) than in rhodopsin and D₂ or CB₁ receptors (n = 6). Thus, this junction in D₂ or CB₁ receptors was modeled as in rhodopsin (PDB codes 1GZM and 2Z73) (25, 26). The unambiguous assignment of the TM boundaries to a particular position is not possible. However, we have assumed that TM5 of A_{2A} extends to position Arg²⁰⁶(5.67) as shown in the crystal structure (20), and TM5 of D₂ extends to position Arg²²⁰(5.69) according to the β₂-based homology model (21, 22). These definitions of TM5 cause Arg²⁰⁵(5.66)–Arg²⁰⁶(5.67) of the A_{2A} receptor and ²¹⁵(5.64)VLR-RRRKRVN²²⁴ of the D₂ receptor to be located at the end of TM5 in the cytoplasm. In contrast, the Swiss Protein Database assigns these epitopes of A_{2A} and D₂ in IL3. The crystal structure of squid rhodopsin (PDB code 2Z73) has shown that in addition to the conserved amphipathic Hx8 that runs parallel to the membrane, the C terminus expands toward TM6 (25). However, the structural homology, among GPCRs, probably does not extend to this C-tail domain because of its high variability in length and amino acid composition among the members of the family. This C-tail is formed by 59 amino acids in the CB₁ receptor (Ser⁴¹⁴–Leu⁴⁷²), only 1 amino acid in the D₂ receptor (Cys⁴⁴³), and 104 amino acids in the A_{2A} receptor (Arg³⁰⁹–Ser⁴¹²). Nevertheless, Ser⁴¹⁴–Asn⁴³⁷ of the CB₁ receptor and Arg³⁰⁹–Gly³³⁰ of the A_{2A} receptor, forming part of this C-tail sequence, were modeled, in an arbitrary manner, based on the structure of squid rhodopsin.

Computational Models of Receptor Heteromers—Cysteine cross-linking experiments have suggested that receptor oligomerization involves the surfaces of TM1, -4, and/or -5 (10, 12, 13). Thus, the structures of receptor heteromers were modeled in such a manner that substituted cysteines at position 1.35 could be cross-linked (TM1–TM1) (13); or positions 4.41, 4.44, 4.48, 4.51, and 4.59 (TM4–TM4^{invag}) (12); or positions 4.50, 4.54, and 4.58 (TM4–TM4^{ago}) (12); or position 5.41 (TM5–TM5) (12).

RESULTS

Quaternary Structure of the A_{2A}-CB₁-D₂ Receptor Heteromer—An obvious initial question about receptor heteromers made up of three different receptors is whether each receptor interacts with the other two or not, *i.e.* if they form a triangular or linear arrangement. As in a prior report (5), we first demonstrated the

Quaternary Structure of Receptor Heteromers

ability of A_{2A} -*Rluc*, D_2 -GFP², and CB_1 -YFP receptors to form heteromers by determining the SRET saturation curve in transfected HEK-293T cells (Fig. 1*a*). In the same experimental preparation, we found significant BRET² and FRET signals between the A_{2A} -*Rluc*- D_2 -GFP² receptor pair and the D_2 -GFP²- CB_1 -YFP receptor pair, respectively (Fig. 1*b*). Furthermore, we also detected by BRET¹ assays a positive transfer of energy between A_{2A} -*Rluc* and CB_1 -YFP receptors (Fig. 1*b*). These data and the positive SRET signal (Fig. 1*a*) in cells co-expressing A_{2A} -*Rluc*, D_2 -GFP², and CB_1 -YFP receptors suggest a triangular arrangement between the three receptors (Fig. 1*c*). In fact, taking into account the correlation between FRET efficiency and acceptor/donor distances and that *Rluc*, GFP², and YFP are fused to the end of the C terminus of the receptors, the distance between BRET donors and acceptors can be approximated (17). Considering the high FRET efficiency between D_2 -GFP² and CB_1 -YFP receptors ($36 \pm 3\%$), the range of the distance between GFP² and YFP in the heteromer is estimated to be 5.7–6.1 nm. Thus, a linear arrangement of the three receptors could give a positive SRET signal but a very much reduced or even nonsignificant BRET¹ signal between A_{2A} -*Rluc* and CB_1 -YFP receptors, because there is a rapid dissipation of the energy transfer (to the 6th power of the distance). Therefore, assuming that the heterotrimer is the minimal unit, only a triangular arrangement of monomers (Fig. 1*c*) would make both SRET (Fig. 1*a*) and BRET¹ (Fig. 1*b*) possible between A_{2A} -*Rluc* and CB_1 -YFP receptors.

Multiple Electrostatic Interactions in A_{2A} - CB_1 - D_2 Receptor Heteromers—The amino acid sequence of the human CB_1 receptor contains two highly conserved epitopes with two adjacent Thr and Ser residues (supplemental Table 1), which have a high probability of CK1/2-dependent phosphorylation (Swiss Protein Database “Net Phos” program (27)). They are located in the distal portion of the C terminus (CT) of the CB_1 receptor (Thr⁴⁶⁷ and Ser⁴⁶⁸) and in the middle portion of intracellular loop (IL) 3 (Thr³²¹ and Ser³²²). The initial working hypothesis was that these CB_1 receptor epitopes, with high probability of phosphorylation, would be relevant in determining the quaternary structure of the A_{2A} - CB_1 - D_2 receptor heteromer, by establishing electrostatic interactions with Arg-rich epitopes located in the A_{2A} and D_2 receptors.

Electrostatic Interaction between Phosphorylated Thr⁴⁶⁷-Ser⁴⁶⁸ in the C Terminus of the CB_1 Receptor and Arg²⁰⁵(5.66)-Arg²⁰⁶(5.67) in the Cytoplasm at the End of Transmembrane Helix 5 of the A_{2A} Receptor—We first looked at possible alterations in heteromerization between CB_1 and A_{2A} and between CB_1 and D_2 receptor in cells co-expressing a mutant CB_1 receptor in which Thr⁴⁶⁷(CT) and Ser⁴⁶⁸(CT) were replaced by Ala ($CB_1^{A467-A468}$ receptor). In cells co-expressing A_{2A} -*Rluc* and $CB_1^{A467-A468}$ -YFP receptors, there was a reduction of BRET¹ values when compared with those obtained with cells expressing A_{2A} -*Rluc* and CB_1 -YFP (Fig. 2*a*). On the other hand, these mutations did not modify the FRET values between D_2 -GFP² and $CB_1^{A467-A468}$ -YFP, when compared with cells expressing D_2 -GFP² and CB_1 -YFP (Fig. 2*b*). This mutated CB_1 receptor and all the mutant receptors described below were shown to be well expressed at the membrane level (results not shown). Furthermore, the fact that the mutated CB_1 receptor selectively

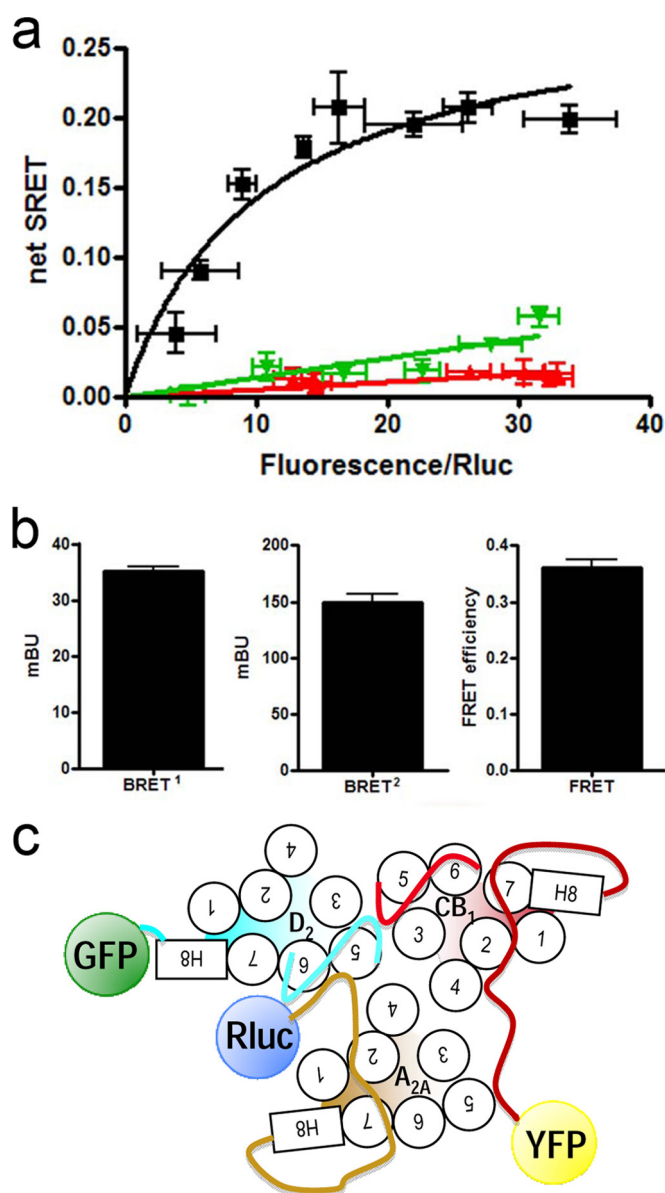


FIGURE 1. A_{2A} - CB_1 - D_2 receptor heteromerization in living cells. Assays were performed 48 h post-transfection in cells expressing A_{2A} -*Rluc* receptor (1 μ g of cDNA; \sim 100,000 luminescence units), D_2 -GFP² receptor (3 μ g of cDNA; \sim 6,000 fluorescence units), and increasing amounts of CB_1 -YFP receptor cDNA (8,000–18,000 fluorescence units). In each sample fluorescence or luminescence was measured before every experiment to confirm similar donor expressions while monitoring the increased acceptor expression. *a* and *b*, aliquots of these cells were used. *a*, net SRET² was obtained by monitoring the YFP fluorescence emission after DeepBlueC addition, with subtraction of the value obtained with cells expressing the same amount of A_{2A} -*Rluc* and D_2 -GFP² receptors. SRET saturation curves (black) were obtained for the coupling of A_{2A} -*Rluc*, D_2 -GFP², and CB_1 -YFP receptors, although negligible and linear SRET was obtained in cells expressing equivalent amounts of A_{2A} -*Rluc*, D_2 -GFP², and 5HT_{2B}-YFP receptors (green) or D_4 -*Rluc*, A_{2A} -GFP², and CB_1 -YFP receptors (red). SRET data are expressed as means \pm S.D. of 5–8 different experiments grouped as a function of the amount of SRET acceptor. *b*, BRET¹ was obtained by monitoring the YFP fluorescence emission after coelenterazine H addition, with subtraction of the value obtained with cells expressing the same amount of A_{2A} -*Rluc* receptor. BRET² was obtained by monitoring the emission of GFP² fluorescence after DeepBlueC addition, with subtraction of the value obtained with cells expressing the same amount of A_{2A} -*Rluc* receptors. FRET was measured by monitoring the emission of YFP fluorescence after excitation of GFP² at 400 nm. Data are expressed as the mean \pm S.E. of 5–8 independent experiments performed in duplicate. Linear unmixing of the emission signals was applied to BRET² and FRET values (*b*) and for YFP quantification in saturation curves (*a*). *c*, schematic representation of the putative triangular quaternary structure of the A_{2A} - CB_1 - D_2 receptor heteromer. mBU, milli-BRET unit.

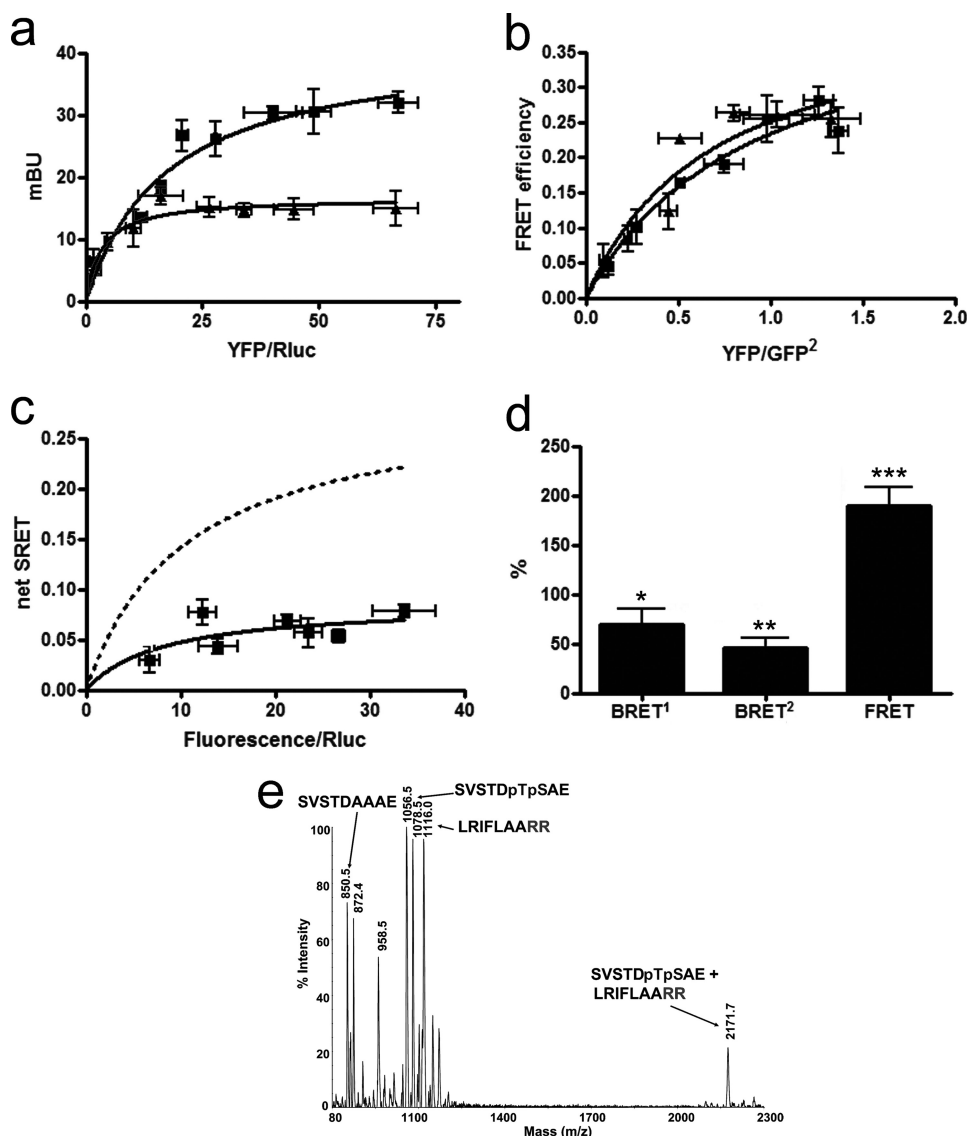


FIGURE 2. A_{2A} -CB₁^{A467-A468}-D₂ receptor heteromerization in living cells. Assays were performed 48 h post-transfection in cells expressing the following: *a*, A_{2A} -Rluc receptor (1 μ g of cDNA; ~100,000 luminescence units) and increasing amounts of cDNA of the CB₁-YFP or CB₁^{A467-A468}-YFP receptors (8,000–18,000 fluorescence units); *mBu*, milli-BRET unit. *b*, D₂-GFP² (3 μ g of the cDNA; ~6,000 fluorescence units) and increasing amounts of the cDNA for CB₁-YFP or CB₁^{A467-A468}-YFP; *c* and *d*, A_{2A} -Rluc receptor (1 μ g of cDNA; ~100,000 luminescence units), D₂-GFP² receptor (3 μ g of the cDNA; ~6,000 fluorescence units), and increasing amounts of cDNA of the CB₁^{A467-A468}-YFP receptor (8,000–18,000 fluorescence units). In each sample, fluorescence or luminescence was measured before every experiment to confirm similar donor expressions while monitoring the increased acceptor expression. *a*, BRET¹ saturation curves for the A_{2A} -Rluc-CB₁-YFP receptor pair (squares) and for the A_{2A} -Rluc-CB₁^{A467-A468}-YFP receptor pair (triangles) were obtained by monitoring the YFP fluorescence emission after coelenterazine H addition, with subtraction of the value obtained with cells expressing the same amount of A_{2A} -Rluc receptor. Data are expressed as means \pm S.D. of five different experiments grouped as a function of the amount of BRET¹ acceptor. *b*, FRET saturation curves for the D₂-GFP²-CB₁-YFP receptor pair (triangles) and for the D₂-GFP²-CB₁^{A467-A468}-YFP receptor pair (squares) were obtained by monitoring the YFP fluorescence emission at 530 nm after excitation of GFP² at 400 nm, with subtraction of the value obtained with cells expressing the same amount of donor protein. Data are expressed as means \pm S.D. of seven different experiments grouped as a function of the amount of FRET acceptor. *c*, net SRET² was obtained by monitoring the emission of YFP fluorescence after DeepBlueC addition, with subtraction of the value obtained with cells expressing the same amount of A_{2A} -Rluc and D₂-GFP² receptors. SRET saturation curves (solid line) were obtained for the coupling of A_{2A} -Rluc, D₂-GFP², and CB₁^{A467-A468}-YFP receptors and compared with the curve obtained for the coupling of A_{2A} -Rluc, D₂-GFP², and CB₁-YFP receptors (dotted line, see Fig. 1). SRET data are expressed as means \pm S.D. of five different experiments grouped as a function of the amount of SRET acceptor. *d*, BRET¹, BRET², and FRET were measured as indicated in Fig. 1 legend. Data are expressed as % of values obtained in cells expressing A_{2A} -Rluc, D₂-GFP², and CB₁-YFP receptors (control, Fig. 1b), in mean \pm S.E. of five independent experiments performed in duplicate. One-way ANOVA followed by Bonferroni test showed significant increases or decreases with respect to the control (*, $p < 0.05$; **, $p < 0.01$; ***, $p < 0.005$). Linear unmixing of the emission signals was applied to the data for BRET² and FRET values (*b* and *d*) and for YFP quantification in saturation curves (*a* and *c*). *e*, the spectrum of a mixture of the following three peptides SVSTDAAAE, SVSTDpTpSAE, and LRIFLAARR, shows only one noncovalent complex between SVSTDpTpSAE and LRIFLAARR at 2171.7 atomic mass units (see text).

altered the RET signal when co-expressed with A_{2A} but not with the D₂ receptors demonstrates that the results cannot be explained by changes in the membrane expression of the mutant receptor or its putative partner. These results therefore show that Thr⁴⁶⁷(CT) and Ser⁴⁶⁸(CT) of the CB₁ receptor are involved in the molecular interaction with the A_{2A} receptor in the A_{2A} -CB₁ receptor heteromer. The existence of measurable BRET¹ values in cells co-expressing A_{2A} -Rluc and CB₁^{A467-A468}-YFP receptors indicate that the CB₁^{A467-A468} receptor is still able to interact physically with the A_{2A} receptor and that other domains, most likely TM domains (see Introduction), are also involved in A_{2A} -CB₁ receptor heteromerization. This CT epitope of the CB₁ receptor was also able to interact with the A_{2A} receptor in the A_{2A} -CB₁-D₂ receptor heteromer, as deduced from the low SRET values obtained when CB₁^{A467-A468}-YFP receptor was co-expressed with A_{2A} -Rluc and D₂-GFP² receptors (Fig. 2c). Furthermore, in cells expressing CB₁^{A467-A468}-YFP, A_{2A} -Rluc, and D₂-GFP² receptors, BRET¹ values between A_{2A} -Rluc and CB₁^{A467-A468}-YFP receptors and BRET² values between A_{2A} -Rluc and D₂-GFP² receptors were significantly reduced, and FRET values between D₂-GFP² and CB₁^{A467-A468}-YFP receptors were increased relative to cells expressing nonmutated receptors (Fig. 2d). Because the bioluminescent or fluorescent proteins are fused to the CT of the receptors, these results indicate that expression of CB₁^{A467-A468}-YFP receptors induced a modification of the quaternary structure of the A_{2A} -CB₁-D₂ heteromer, with separation of the CT of CB₁ and A_{2A} receptors and A_{2A} and D₂ receptors and approximation of the CT of CB₁ and D₂ receptors.

We then looked for the presence of adjacent Arg residues in intracellular domains of the A_{2A} receptor that could potentially interact with the phosphorylated Thr⁴⁶⁷(CT) and Ser⁴⁶⁸(CT) of CB₁

Quaternary Structure of Receptor Heteromers

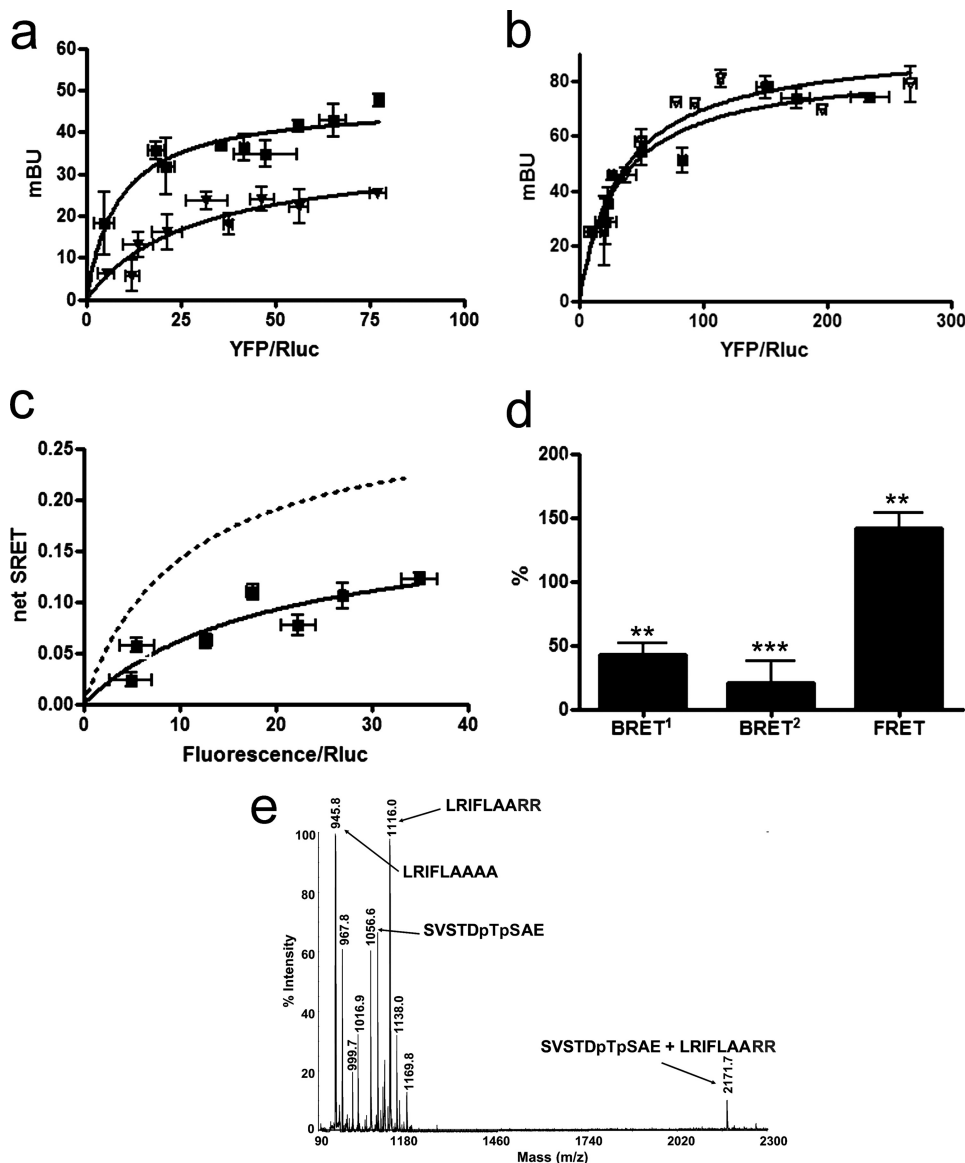


FIGURE 3. $A_{2A}^{A205-A206}$ - CB_1 - D_2 receptor heteromerization in living cells. Assays were performed 48 h post-transfection in cells expressing the following: *a*, A_{2A} -*Rluc* or $A_{2A}^{A205-A206}$ -*Rluc* receptors (1 or 0.8 μ g of cDNA respectively; \sim 100,000 luminescence units) and increasing amounts of the cDNA of the CB_1 -YFP receptor (8,000–18,000 fluorescence units). *mBu*, milli-BRET unit. *b*, A_{2A} -*Rluc* or $A_{2A}^{A205-A206}$ -*Rluc* (1 or 0.8 μ g of cDNA, respectively; \sim 100,000 luminescence units) and increasing amounts of the cDNA of D_2 -YFP. *c* and *d*, $A_{2A}^{A205-A206}$ -*Rluc* receptor (1 μ g of cDNA; \sim 100,000 luminescence units), D_2 -GFP² receptor (3 μ g of the cDNA; \sim 6,000 fluorescence units), and increasing amounts of cDNA of the CB_1 -YFP receptor (8,000–18,000 fluorescence units). In each sample fluorescence or luminescence was measured before every experiment to confirm similar donor expressions while monitoring the increased acceptor expression. *a*, BRET¹ saturation curves for the A_{2A} -*Rluc*- CB_1 -YFP receptor pairs (squares) and for the $A_{2A}^{A205-A206}$ -*Rluc*- CB_1 -YFP receptor pair (triangles) were obtained by monitoring the YFP fluorescence emission after coelenterazine H addition, with subtraction of the value obtained with cells expressing the same amount of donor. Data are expressed as means \pm S.D. of five different experiments grouped as a function of the amount of BRET¹ acceptor. *b*, BRET¹ saturation curves for the A_{2A} -*Rluc*- D_2 -YFP receptor pairs (triangles) and for the $A_{2A}^{A205-A206}$ -*Rluc*- D_2 -YFP receptor pair (squares) were obtained by monitoring the YFP fluorescence emission after coelenterazine H addition, with subtraction of the value obtained with cells expressing the same amount of donor. Data are expressed as means \pm S.D. of five different experiments grouped as a function of the amount of BRET¹ acceptor. *c*, net SRET² was obtained by monitoring the YFP fluorescence emission after DeepBlueC addition, with subtraction of the value obtained with cells expressing the same amount of $A_{2A}^{A205-A206}$ -*Rluc* and D_2 -GFP² receptors. SRET saturation curves (solid line) were obtained for the coupling of $A_{2A}^{A205-A206}$ -*Rluc*, D_2 -GFP², and CB_1 -YFP receptors and compared with the curve obtained for the coupling of A_{2A} -*Rluc*, D_2 -GFP², and CB_1 -YFP receptors (dotted line, see Fig. 1). SRET data are expressed as means \pm S.D. of five different experiments grouped as a function of the amount of SRET acceptor. *d*, BRET¹, BRET², and FRET were measured as indicated in Fig. 1 legend. Data are expressed as % of values obtained in cells expressing A_{2A} -*Rluc*, D_2 -GFP², and CB_1 -YFP receptors (control, Fig. 1b), in mean \pm S.E. of five independent experiments performed in duplicate. One-way ANOVA followed by Bonferroni test showed significant increases or decreases with respect to the control (**, $p < 0.01$; ***, $p < 0.005$). Linear unmixing of the emission signals was applied to the data for BRET² and FRET values (*d*) and for YFP quantification in saturation curves (*a*–*c*). *e*, spectrum of a mixture of the following three peptides LRIFLAAAA, LRIFLAARR, and SVSTDpTpSAE, shows only one NCX between SVSTDpTpSAE and LRIFLAARR at 2171.7 atomic mass units (see text).

receptor via electrostatic interactions. We found a highly conserved motif, Arg²⁰⁵(5.66)–Arg²⁰⁶(5.67) (supplemental Table 1), located in the cytoplasm at the end of TM5, according to the crystal structure (see “Experimental Procedures”). Mass spectrometric analysis demonstrated that a synthetic peptide corresponding to this A_{2A} receptor epitope, ¹⁹⁸LRIFLAARR²⁰⁶, and a phosphorylated peptide corresponding to the CT of the CB_1 receptor epitope, ⁴⁶²SVSTDpTpSAE⁴⁷⁰, form stable noncovalent complexes, and the Ala-containing peptides LRIFLAAAA and SVSTDAAAAE do not (Figs. 2e and 3e). We then investigated whether the A_{2A} receptor epitope containing adjacent Arg could be involved in A_{2A} - CB_1 receptor heteromerization by using a mutant A_{2A} receptor in which Arg²⁰⁵(5.66)–Arg²⁰⁶(5.67) were replaced by Ala ($A_{2A}^{A205-A206}$ receptor). Cells co-expressing $A_{2A}^{A205-A206}$ -*Rluc* and CB_1 -YFP receptors showed lower BRET¹ values than those expressing WT receptors (Fig. 3a). On the other hand, the BRET¹ values between $A_{2A}^{A205-A206}$ -*Rluc* and D_2 -YFP receptors were similar to the values between A_{2A} -*Rluc* and D_2 -YFP receptors (Fig. 3b). Hence, the quaternary structure of the A_{2A} - CB_1 receptor heteromer depends on an electrostatic interaction between epitopes located in the CT of the CB_1 receptor and in the cytoplasm at the end of TM5 of the A_{2A} receptor. Furthermore, this electrostatic interaction is also involved in A_{2A} - CB_1 - D_2 receptor heteromerization (Fig. 3, c and d). In fact, low SRET values were obtained when the $A_{2A}^{A205-A206}$ -*Rluc* receptor was co-transfected with D_2 -GFP² and CB_1 -YFP receptors (Fig. 3c). In cells co-expressing $A_{2A}^{A205-A206}$ -*Rluc*, D_2 -GFP², and CB_1 -YFP receptors, BRET¹ and BRET² between the heteromer partners were significantly reduced, and FRET values between D_2 -GFP² and CB_1 -YFP receptors were increased, compared with cells co-expressing nonmutated receptors (Fig. 3d). Significantly,

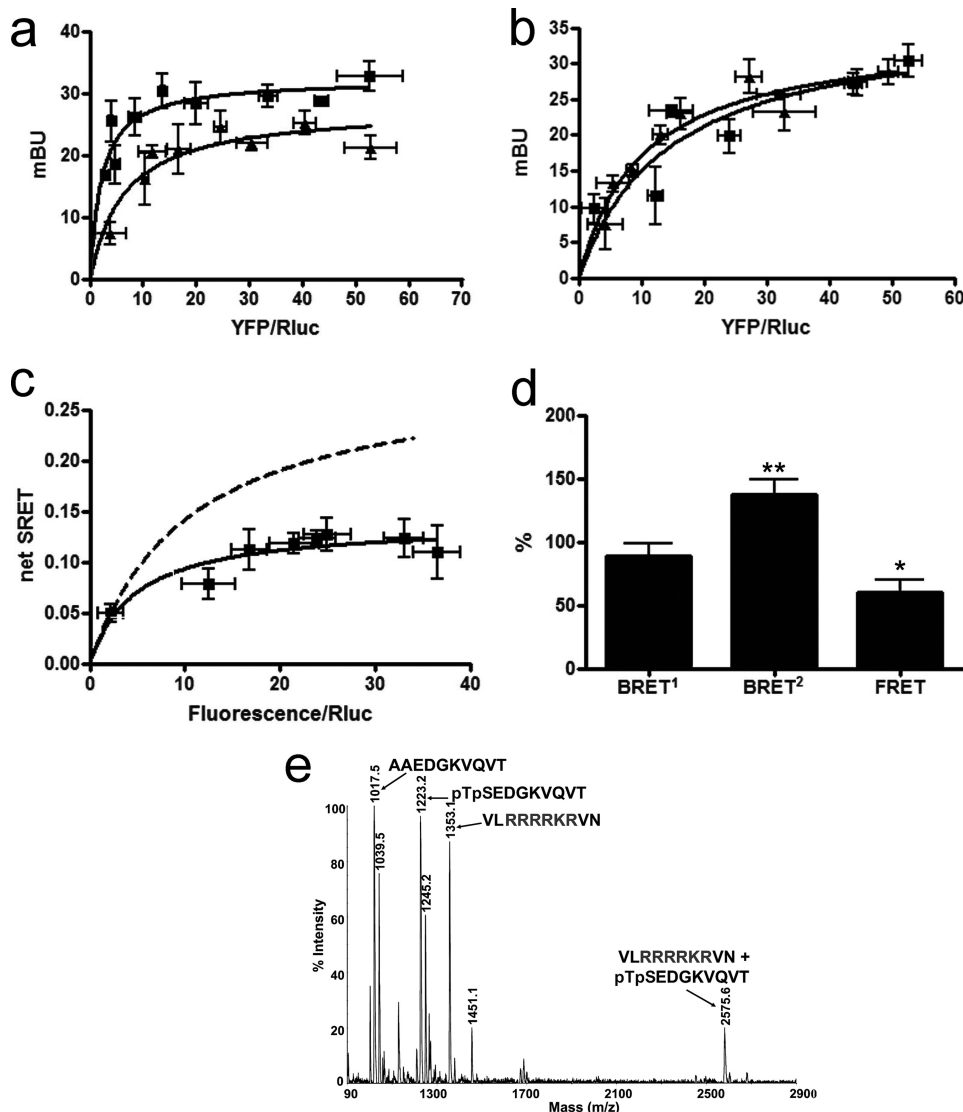


FIGURE 4. A_{2A} - $CB_1^{A321-A322}$ - D_2 receptor heteromerization in living cells. Assays were performed 48 h post-transfection in cells expressing the following: *a*, D_2 - $Rluc$ receptor ($1 \mu\text{g}$ of cDNA; $\sim 100,000$ luminescence units) and increasing amounts of the cDNA for CB_1 -YFP or $CB_1^{A321-A322}$ -YFP receptors (8,000–18,000 fluorescence units); *b*, A_{2A} - $Rluc$ ($1 \mu\text{g}$ of cDNA; $\sim 100,000$ luminescence units) and increasing amounts of the cDNA for CB_1 -YFP or $CB_1^{A321-A322}$ -YFP; *c* and *d*, A_{2A} - $Rluc$ receptor ($1 \mu\text{g}$ of cDNA; $\sim 100,000$ luminescence units), D_2 -GFP² receptor ($3 \mu\text{g}$ of the cDNA; $\sim 6,000$ fluorescence units), and increasing amounts of cDNA of the $CB_1^{A321-A322}$ -YFP receptor (8,000–18,000 fluorescence units). In each sample fluorescence or luminescence was measured before every experiment to confirm similar donor expressions while monitoring the increased acceptor expression. *a*, BRET¹ saturation curves for the D_2 - $Rluc$ - CB_1 -YFP receptor pair (squares) and for D_2 - $Rluc$ - $CB_1^{A321-A322}$ -YFP receptor pair (triangles) were obtained by monitoring the YFP fluorescence emission after coelenterazine H addition, with subtraction of the value obtained with cells expressing the same amount of A_{2A} - $Rluc$ receptor. Data are expressed as means \pm S.D. of six different experiments grouped as a function of the amount of BRET¹ acceptor. *b*, BRET¹ saturation curves for the A_{2A} - $Rluc$ - CB_1 -YFP receptor pair (triangles) and for A_{2A} - $Rluc$ - $CB_1^{A321-A322}$ -YFP receptor pair (squares) were obtained by monitoring the YFP fluorescence emission after coelenterazine H addition, with subtraction of the value obtained with cells expressing the same amount of A_{2A} - $Rluc$ receptor. Data are expressed as means \pm S.D. of six different experiments grouped as a function of the amount of BRET¹ acceptor. *c*, net SRET² was obtained by monitoring the YFP fluorescence emission after DeepBlueC addition, with subtraction of the value obtained with cells expressing the same amount of A_{2A} - $Rluc$ and D_2 -GFP² receptors. SRET saturation curves (solid line) were obtained for the coupling of A_{2A} - $Rluc$, D_2 -GFP², and $CB_1^{A321-A322}$ -YFP receptors and compared with the curve obtained for the coupling of A_{2A} - $Rluc$, D_2 -GFP², and CB_1 -YFP receptors (dotted line, see Fig. 1). SRET data are expressed as means \pm S.D. of six different experiments grouped as a function of the amount of SRET acceptor. *d*, BRET¹, BRET², and FRET were measured as indicated in Fig. 1b legend. Data are expressed as percent of values obtained in cells expressing A_{2A} - $Rluc$, D_2 -GFP², and CB_1 -YFP receptors (control, Fig. 1b), in mean \pm S.E. of six independent experiments performed in duplicate. One-way ANOVA followed by Bonferroni test showed significant increases or decreases with respect to the control (*, $p < 0.05$; **, $p < 0.01$). Linear unmixing of the emission signals was applied to the data for BRET² and FRET values (*d*) and for YFP quantification in saturation curves (*a*–*c*). *e*, the spectrum of a mixture of the following three peptides AAEDGKQVQT, pTpSEDGKQVQT, and VLRRRRKRNVN shows only one NCX between pTpSEDGKQVQT and VLRRRRKRNVN at 2575.6 atomic mass units (see text). *mBu*, milli-BRET unit.

this outcome is qualitatively the same as the one shown in Fig. 2*d* with $CB_1^{A467-A468}$ -YFP receptor, as it would be expected if both mutants disrupt the same intermolecular interaction.

Electrostatic Interaction between Phosphorylated Thr³²¹-Ser³²² in Intracellular Loop 3 of the CB₁ Receptor and an Arg-rich Epitope in Intracellular Loop 3 of the D₂ Receptor—Because the Thr⁴⁶⁷(CT)-Ser⁴⁶⁸(CT)-containing epitope of the CB_1 receptor was found to interact with Arg²⁰⁵(5.66)–Arg²⁰⁶(5.67) of the A_{2A} receptor, it was expected that Thr³²¹(IL3)–Ser³²²(IL3) of the CB_1 receptor could interact with the D_2 receptor. In fact, when co-expressing the mutant $CB_1^{A321-A322}$ -YFP and D_2 - $Rluc$ receptors, the BRET¹ energy transfer between $Rluc$ and YFP was reduced when compared with BRET¹ values obtained with CB_1 -YFP and D_2 - $Rluc$ receptors (Fig. 4*a*). On the other hand, the BRET¹ values obtained in cells expressing $CB_1^{A321-A322}$ -YFP and A_{2A} - $Rluc$ receptors were similar to those obtained with cells expressing CB_1 -YFP and A_{2A} - $Rluc$ (Fig. 4*b*). These results therefore show that the Thr³²¹(IL3)–Ser³²²(IL3) motif of the CB_1 receptor is selectively involved in the intermolecular interactions with the D_2 receptor in the CB_1 - D_2 receptor heteromer. The fact that BRET¹ is still measurable between $CB_1^{A321-A322}$ -YFP and D_2 - $Rluc$ receptors indicates that, once more, other epitopes are also involved in CB_1 - D_2 receptor heteromerization. Also, the same Thr³²¹(IL3)–Ser³²²(IL3) epitope of the CB_1 receptor interacted with the D_2 receptor in the A_{2A} - CB_1 - D_2 receptor heteromer. Compared with nonmutated receptors, co-expression of $CB_1^{A321-A322}$ -YFP receptor with A_{2A} - $Rluc$ and D_2 -GFP² receptors showed a reduction in SRET values (Fig. 4*c*), and FRET values were significantly decreased, and BRET² values were increased, whereas BRET¹ values were not modified (Fig. 4*d*). This suggests that replacement of

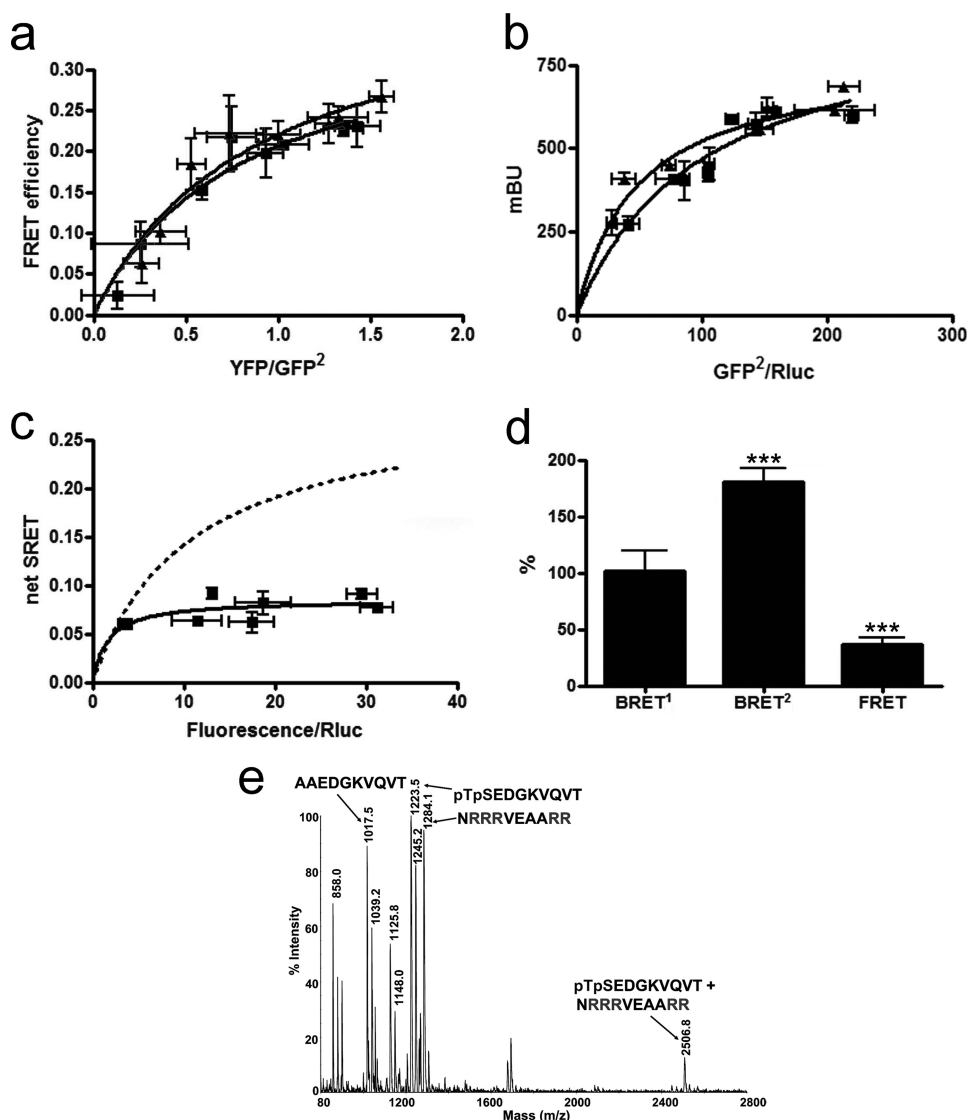


FIGURE 5. A_{2A} -CB₁-D₂₅ receptor heteromerization in living cells. Assays were performed 48 h post-transfection in cells expressing the following: *a*, D₂₅-GFP² receptor (1.5 μ g of cDNA; \sim 5,000 fluorescence units) or D₂-GFP² receptor (2 μ g of cDNA; \sim 5,000 luminescence units), and increasing amounts of cDNA of CB₁-YFP receptor (8,000–18,000 fluorescence units); *b*, A_{2A} -Rluc (1 μ g of cDNA; \sim 100,000 luminescence units) and increasing amounts of cDNA for D₂-GFP² or D₂₅-GFP²; *c* and *d*, A_{2A} -Rluc receptor (1 μ g of cDNA; \sim 100,000 luminescence units), D₂₅-GFP² receptor (3 μ g of the cDNA; \sim 6,000 fluorescence units) and increasing amounts of the cDNA for CB₁-YFP receptor (8,000–18,000 fluorescence units). *mBu*, milli-BRET unit. In each sample fluorescence or luminescence was measured before every experiment to confirm similar donor expressions while monitoring the increased acceptor expression. *a*, FRET saturation curves for the D₂-GFP²-CB₁-YFP receptor pair (squares) and for D₂₅-GFP²-CB₁-YFP receptor pair (triangles) were obtained by monitoring the YFP fluorescence emission at 530 nm after excitation of GFP² at 400 nm, with subtraction of the value obtained with cells expressing the same amount of donor protein. Data are expressed as means \pm S.D. of seven different experiments grouped as a function of the amount of FRET acceptor. *b*, BRET² saturation curves for the A_{2A} -Rluc-D₂-GFP² receptor pair (triangles) and for A_{2A} -Rluc-D₂₅-GFP² receptor pair (squares) were obtained by monitoring the YFP fluorescence emission after DeepBlueC addition, with subtraction of the value obtained with cells expressing the same amount of A_{2A} -Rluc receptor. Data are expressed as means \pm S.D. of six different experiments grouped as a function of the amount of BRET² acceptor. *c*, net SRET² was obtained by monitoring the YFP fluorescence emission after DeepBlueC addition, with subtraction of the value obtained with cells expressing the same amount of A_{2A} -Rluc and D₂₅-GFP² receptors. SRET saturation curves (solid line) were obtained for the coupling of A_{2A} -Rluc, D₂₅-GFP², and CB₁-YFP receptors and compared with the curve obtained for the coupling of A_{2A} -Rluc, D₂-GFP², and CB₁-YFP receptors (dotted line, see Fig. 1). SRET data are expressed as means \pm S.D. of five different experiments grouped as a function of the amount of SRET acceptor. *d*, BRET¹, BRET², and FRET were measured as indicated in Fig. 1 legend. Data are expressed as % of values obtained in cells expressing A_{2A} -Rluc, D₂-GFP², and CB₁-YFP receptors (control, Fig. 1b), in mean \pm S.E. of five independent experiments performed in duplicate. One-way ANOVA followed by Bonferroni test showed significant increases or decreases with respect to the control (***, $p < 0.005$). Linear unmixing of the emission signals was applied to the data for BRET² and FRET values (*a*, *b*, and *d*) and for YFP quantification in saturation curves (*a* and *c*). *e*, spectrum of a mixture of the following three peptides AAEDGKVVQT, pTpSEDGKVVQT, and NRRRVEAARR, shows only one NCX between pTpSEDGKVVQT and NRRRVEAARR at 2506.8 atomic mass units (see text).

Thr³²¹(IL3) and Ser³²²(IL3) by Ala in CB₁ receptor induces a modification of the quaternary structure of the A_{2A} -CB₁-D₂ receptor heteromer with separation of the CT of the CB₁ and D₂ receptors and an approximation of the CT of the D₂ and A_{2A} receptors. Thus, CB₁ receptor uses two different CK1/2-dependent phosphorylatable epitopes, located in their CT (Thr⁴⁶⁷-Ser⁴⁶⁸) and IL3 (Thr³²¹-Ser³²²) domains, to establish simultaneous electrostatic interactions with the A_{2A} and D₂ receptors, respectively, in the A_{2A} -CB₁-D₂ receptor heteromer.

Next step was finding out which intracellular epitope of the D₂ receptor is involved in CB₁-D₂ receptor heteromerization. D₂ receptor contains two highly conserved Arg-rich epitopes (supplemental Table 1), ²¹⁵(5.64)VLR^{RRRKR}VN²²⁴, located at the end of TM5 in the cytoplasm (according to the homology modeling using the β_2 -adrenergic receptor as a template; see under "Experimental Procedures"), and ²⁶⁶NRRRVEAARR²⁷⁵, in the middle of IL3. Because the VLR^{RRRKR}VN epitope is most probably involved in A_{2A} -D₂ receptor heteromerization (28, 29), we explored the possibility that IL3 of the D₂ receptor could interact with IL3 of the CB₁ receptor (phosphorylated Thr³²¹-Ser³²²). The D₂ short isoform (D₂₅), an alternative splicing that lacks 29 amino acid residues of IL3 (30), including ²⁶⁶NRRRVEAARR²⁷⁵, was used. SRET values were clearly reduced when D₂₅-GFP² receptor was co-expressed with A_{2A} -Rluc and CB₁-YFP receptors (Fig. 5c). Significantly, the D₂₅ receptor led to the same qualitative modifications of the quaternary structure of the A_{2A} -CB₁-D₂ receptor heteromer as those induced by CB₁^{A321-A322}-YFP receptor (Fig. 5d). Thus, in cells expressing A_{2A} -Rluc, CB₁-YFP, and D₂₅-GFP² receptors, FRET values between D₂₅-GFP² and CB₁-YFP receptors were significantly decreased, whereas BRET² values between A_{2A} -Rluc and D₂₅-GFP²

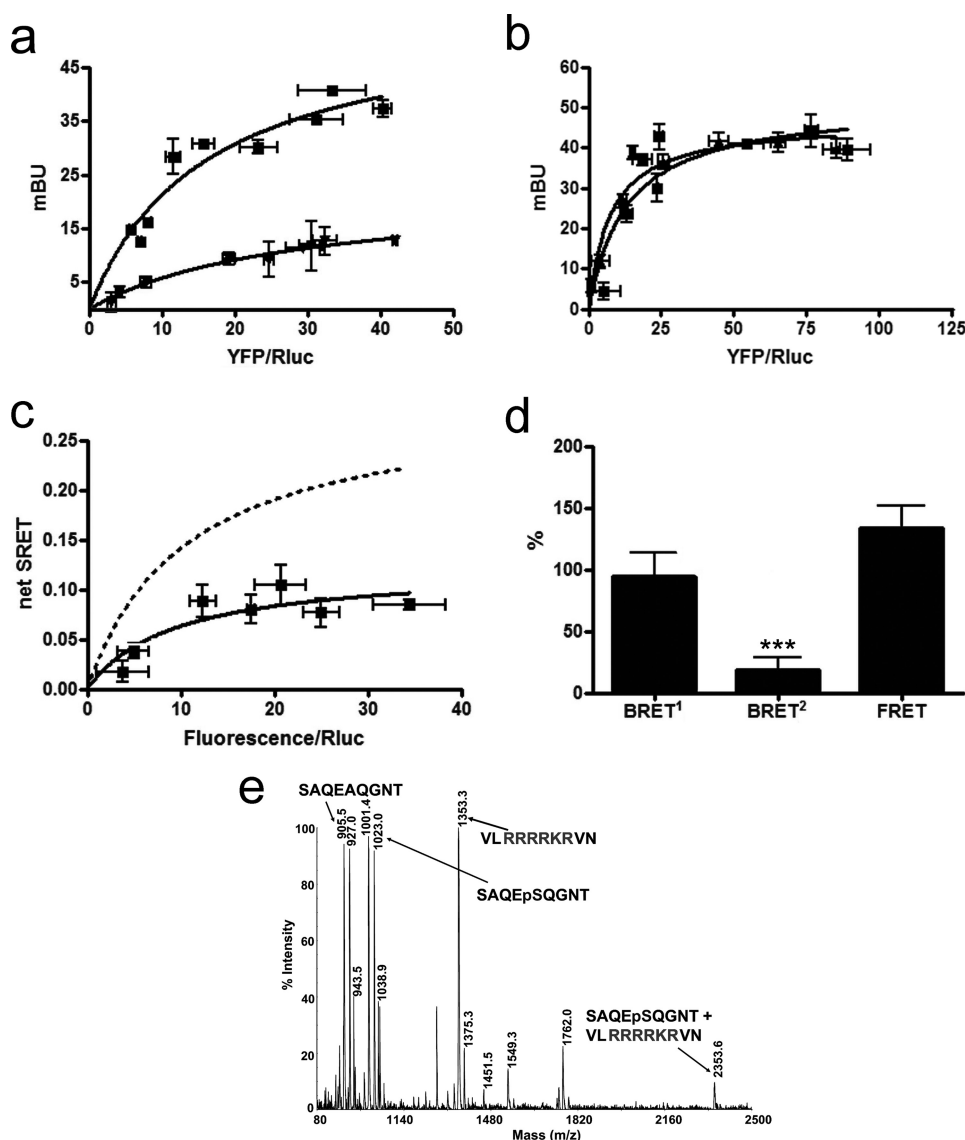


FIGURE 6. A_{2A}^{A374} -CB₁-D₂ receptor heteromerization in living cells. Assays were performed 48 h post-transfection in cells expressing the following: *a*, A_{2A} -Rluc or A_{2A}^{A374} -Rluc receptors (1 or 0.8 μ g of cDNA respectively; \sim 100,000 luminescence units) and increasing amounts of cDNA of the D₂-YFP receptor (8,000–18,000 fluorescence units); *b*, A_{2A} -Rluc or A_{2A}^{A374} -Rluc (1 or 0.8 μ g of cDNA respectively; \sim 100,000 luminescence units) and increasing amounts of the cDNA for CB₁-YFP; *c* and *d*, A_{2A}^{A374} -Rluc receptor (1 μ g of cDNA; \sim 100,000 luminescence units), D₂-GFP² receptor (3 μ g of the cDNA; \sim 6,000 fluorescence units), and increasing amounts of cDNA of CB₁-YFP receptor (8,000–18,000 fluorescence units). In each sample fluorescence or luminescence was measured before every experiment to confirm similar donor expressions while monitoring the increased acceptor expression. *a*, BRET¹ saturation curves for the A_{2A} -Rluc-D₂-YFP receptor pair (squares) and for the A_{2A}^{A374} -Rluc-D₂-YFP receptor pair (triangles) were obtained by monitoring the YFP fluorescence emission after coelenterazine H addition, with subtraction of the value obtained with cells expressing the same amount of donor. Data are expressed as means \pm S.D. of five different experiments grouped as a function of the amount of BRET¹ acceptor. *b*, BRET¹ saturation curves for the A_{2A} -Rluc-CB₁-YFP receptor pair (triangles) and for the A_{2A}^{A374} -Rluc-CB₁-YFP receptor pair (squares) were obtained by monitoring the YFP fluorescence emission after coelenterazine H addition, with subtraction of the value obtained with cells expressing the same amount of donor. Data are expressed as means \pm S.D. of five different experiments grouped as a function of the amount of BRET¹ acceptor. *c*, net SRET² was obtained by monitoring the YFP fluorescence emission after DeepBlueC addition, with subtraction of the value obtained with cells expressing the same amount of A_{2A}^{A374} -Rluc and D₂-GFP² receptors. SRET saturation curves (solid line) were obtained for the coupling of A_{2A}^{A374} -Rluc, D₂-GFP², and CB₁-YFP receptors and compared with the curve obtained for the coupling of A_{2A} -Rluc, D₂-GFP², and CB₁-YFP receptors (dotted line, see Fig. 1). SRET data are expressed as mean \pm S.D. of five different experiments grouped as a function of the amount of SRET acceptor. *d*, BRET¹, BRET², and FRET were measured as indicated in Fig. 1 legend. Data are expressed as % of values obtained in cells expressing A_{2A} -Rluc, D₂-GFP², and CB₁-YFP (control, Fig. 1b) in mean \pm S.E. of five independent experiments performed in duplicate. One-way ANOVA followed by Bonferroni test showed significant increases or decreases with respect to the control (*, $p < 0.05$; **, $p < 0.01$; ***, $p < 0.005$). Linear unmixing of the emission signals was applied to the data for BRET² and FRET values (*e*) and for YFP quantification in saturation curves (*a* and *b*). *e*, spectrum of a mixture of the following three peptides SAQEAQGNT, SAQEpSQGNT, and VLRRRRKRNV shows only one NCX between SAQEpSQGNT and VLRRRRKRNV at 2353.6 atomic mass units (see text). *mBu*, milli-BRET unit.

receptors were increased, and BRET¹ values between A_{2A} -Rluc and CB₁-YFP receptors were not modified, when compared with cells co-expressing A_{2A} -Rluc, D₂-GFP², and CB₁-YFP receptors (Fig. 5*d*). These results indicate that in the A_{2A} -CB₁-D₂ receptor heteromer, CB₁ receptors interact with the Arg-rich domain located in IL3 of the D₂ receptor.

Notably, expression of D_{2S}-GFP² or D₂-GFP² receptors with either CB₁-YFP or A_{2A} -Rluc or receptors gives similar FRET (Fig. 5*a*) or BRET² (Fig. 5*b*) values, respectively. This indicates that in the absence of the ²⁶⁶NRRRVEAARR²⁷⁵ epitope in D_{2S}-GFP², the CB₁ receptor can potentially interact with the other Arg-rich domain, ²¹⁵(5.64)VLR-RRRKRNV²²⁴, present in both isoforms of the D₂ receptor. As expected, mass spectrometric analysis demonstrated that a synthetic peptide of the epitope located in IL3 of the CB₁ receptor (³²¹pTpSEDGKVQVT³³⁰), but not its equivalent Ala-containing peptide (AAEDGKVQVT), formed stable noncovalent complexes with the two Arg-rich epitopes of the D₂ receptor (²¹⁵(5.64)VLR-RRRKRNV²²⁴ and ²⁶⁶NRRRVEAARR²⁷⁵) (Figs. 4*e* and 5*e*).

Electrostatic Interaction between Phosphorylated Ser³⁷⁴ in the C Terminus of the A_{2A} Receptor and an Arg-rich Domain in the Cytoplasm at the End of Transmembrane Helix 5 of the D₂ Receptor—The ²¹⁵(5.64)VLR-RRRKRNV²²⁴ epitope of the D₂ receptor was shown to be involved in A_{2A} -D₂ receptor heteromerization by interacting with the CT domain of the A_{2A} receptor (19, 20). We found a dramatic reduction of BRET¹ values in cells co-expressing a mutant A_{2A} -Rluc receptor, in which Ser³⁷⁴(CT) was replaced by Ala (A_{2A}^{A374} -Rluc receptor), and D₂-YFP receptor (Fig. 6*a*). On the other hand, co-expression of A_{2A}^{A374} -Rluc and CB₁-YFP receptors gave similar BRET¹ values than WT receptors (Fig. 6*b*). These results confirm that Ser³⁷⁴(CT) of the A_{2A} receptor is

Quaternary Structure of Receptor Heteromers

involved in the molecular interaction with the D₂ receptor. Not surprisingly, Ser³⁷⁴(CT) of the A_{2A} receptor was also found to be involved in providing the quaternary structure of the A_{2A}-CB₁-D₂ receptor heteromer. Low SRET values were obtained when A_{2A}^{A374}-Rluc was co-expressed with D₂-GFP² and CB₁-YFP receptors (Fig. 6c), compared with cells co-expressing the nonmutated receptors. From the analysis of BRET¹, BRET², and FRET occurring between partners in cells expressing A_{2A}^{A374}-Rluc, CB₁-YFP, and D₂-GFP² receptors, it was observed that BRET² values were significantly reduced, but FRET and BRET¹ values were not significantly modified (Fig. 6d). These results indicate that the CT-mutated A_{2A} receptor induces a modification of the quaternary structure of the A_{2A}-CB₁-D₂ receptor heteromer, with separation of the CT of the A_{2A} and D₂ receptors. Therefore, the A_{2A} receptor uses a double-Arg motif (Arg²⁰⁵(5.66)-Arg²⁰⁶(5.67)) located in the cytoplasm at the end of transmembrane helix 5 and a CK1/2-dependent phosphorylatable epitope located in CT (Ser³⁷⁴) to establish selective electrostatic interactions with the CB₁ and D₂ receptors, respectively. Hence, mass spectrometric analysis of a mixture of peptides corresponding to the cytoplasmic epitope at the end of TM5 of the D₂ (²¹⁵(5.64)VLRRRRKRVN²²⁴) and the CT epitopes of the A_{2A} receptor (³⁷⁰SAQEpsSQGNT³⁷⁸) and the mutant A_{2A} receptor (³⁷⁰SAQEAQGNT³⁷⁸) resulted in noncovalent complexes between the D₂ and the A_{2A} receptor epitopes, but not in the case of the mutant A_{2A} receptor (Fig. 6e).

Role of Casein Kinase 1/2-mediated Phosphorylation in the Quaternary Structure of A_{2A}-CB₁-D₂ Receptor Heteromer—To demonstrate the actual involvement of casein kinase-induced phosphorylation in the electrostatic interactions between A_{2A}, CB₁, and D₂ receptors in the A_{2A}-CB₁-D₂ receptor heteromer, we studied the effects of co-administration of casein kinase 1 inhibitor IC 261 and casein kinase 2 inhibitor TBAC on SRET saturation experiments in HEK-293T cells co-transfected with A_{2A}-Rluc, D₂-GFP², and CB₁-YFP receptors. As expected, the casein kinase inhibitors significantly decreased SRET values (Fig. 7), supporting a role of casein kinases on maintaining a phosphorylated state of the intracellular domains of A_{2A} and CB₁ receptors involved in A_{2A}-CB₁-D₂ receptor heteromerization.

Computational Model of the Quaternary Structure of the A_{2A}-CB₁-D₂ Receptor Heteromer—Biochemical and biophysical studies have suggested that oligomerization of class A GPCRs primarily involves TM1, -4, and/or -5 (7, 9–15). Thus, the structure of the A_{2A}-CB₁-D₂ receptor heteromer was modeled using the following dimeric interfaces: TM1-TM1, TM4-TM4^{invago}, TM4-TM4^{ago}, and TM5-TM5 (see under “Experimental Procedures”). TM4-TM4^{invago} and TM4-TM4^{ago} stand for the proposed rearrangement of the oligomerization interface that has been observed for the dopamine D₂ receptor upon inverse agonist and agonist binding, respectively (12).

Modeling the CB₁-D₂ Receptor Heteromer—Initially, to discern which of these TM interfaces most favorably permits the proposed electrostatic interaction between phosphorylated Thr³²¹(IL3)-Ser³²²(IL3) of CB₁ and ²⁶⁶NRRRVEAARR²⁷⁵(IL3) of D₂ in the CB₁-D₂ receptor heteromer, all possible dimeric interfaces were constructed (supplemental Fig. 1). It is impor-

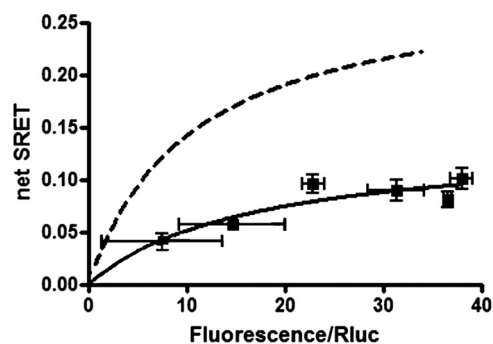


FIGURE 7. A_{2A}-CB₁-D₂ receptor heteromerization in living cells treated with casein kinase 1/2 inhibitors. SRET² saturation experiments were performed 48 h post-transfection in cells expressing A_{2A}-Rluc receptor (1 μg of cDNA), D₂-GFP² receptor (3 μg of cDNA), and increasing amounts of CB₁-YFP receptor cDNA, treated with the casein kinase 1 inhibitor IC 261 (50 μM) and casein kinase 2 inhibitor TBAC (10 μM) as described under “Experimental Procedures.” In each sample fluorescence or luminescence was measured before every experiment to confirm similar donor expressions (~100,000 luminescence units) and similar GFP² fluorescence (~6,000 fluorescence units) while monitoring the increased acceptor expression (8,000–18,000 YFP fluorescence units). Net SRET² was obtained by monitoring the emission of YFP fluorescence after DeepBlueC addition, with subtraction of the value obtained with cells expressing the same amount of receptor Rluc and receptor GFP². SRET² saturation curves (solid lines) were compared with the curve obtained for the coupling of A_{2A}-Rluc, D₂-GFP², and CB₁-YFP receptors in cells not treated with casein kinase inhibitors (dotted line, see Fig. 1). SRET data are expressed as means ± S.D. of five different experiments grouped as a function of the amount of SRET acceptor.

tant to acknowledge the difficulty of modeling IL3 of either CB₁ or D₂ receptors unambiguously (see under “Experimental Procedures”); thus, the exact location of these epitopes in IL3 cannot be determined. Nevertheless, it seems clear to us that the TM1-TM1, TM4-TM4^{invago}, and TM4-TM4^{ago} interfaces position IL3 of CB₁ and D₂ receptors in opposite sides of the TM bundles (supplemental Fig. 1, a–c), which makes the proposed electrostatic interaction difficult. In contrast, the TM5-TM5 interface places IL3 of the CB₁ receptor contiguous to IL3 of the D₂ receptor (supplemental Fig. 1d), facilitating their electrostatic interaction. It thus seems reasonable to propose that the Arg-rich epitope of the D₂ receptor located in the cytoplasm at the end of TM5 is involved in CB₁-D₂ receptor heteromerization.

Modeling the A_{2A}-CB₁ Receptor Heteromer—The A_{2A}-CB₁ receptor heteromer was also modeled through the entire set of TM interfaces (supplemental Fig. 2) to reproduce the electrostatic interaction between phosphorylated Thr⁴⁶⁷-Ser⁴⁶⁸ in the CT of the CB₁ receptor and Arg²⁰⁵(5.66)-Arg²⁰⁶(5.67) in the cytoplasm at the end of TM5 of the A_{2A} receptor. CT of the CB₁ receptor is made of 59 amino acids (Ser⁴¹⁴-Leu⁴⁷²), in addition to the conserved Hx8 that runs parallel to the membrane (Ser⁴⁰¹-Pro⁴¹³). It is thus difficult to determine with precision the position of Thr⁴⁶⁷(CT)-Ser⁴⁶⁸(CT). However, although GPCRs CT vary greatly in length and sequence, we have assumed that the CT of CB₁ unfolds toward TM6 as found in the crystal structure of squid rhodopsin (22). Taking these facts into account, TM4-TM4^{invago}, TM4-TM4^{ago}, and TM5-TM5 interfaces between CB₁ and A_{2A} receptors would allow the electrostatic interaction between Thr⁴⁶⁷(CT)-Ser⁴⁶⁸(CT) and Arg²⁰⁵(5.66)-Arg²⁰⁶(5.67) in the A_{2A} receptor (supplemental Fig. 2, b–d), whereas the TM1-TM1 interface would not (supplemental Fig. 2a).

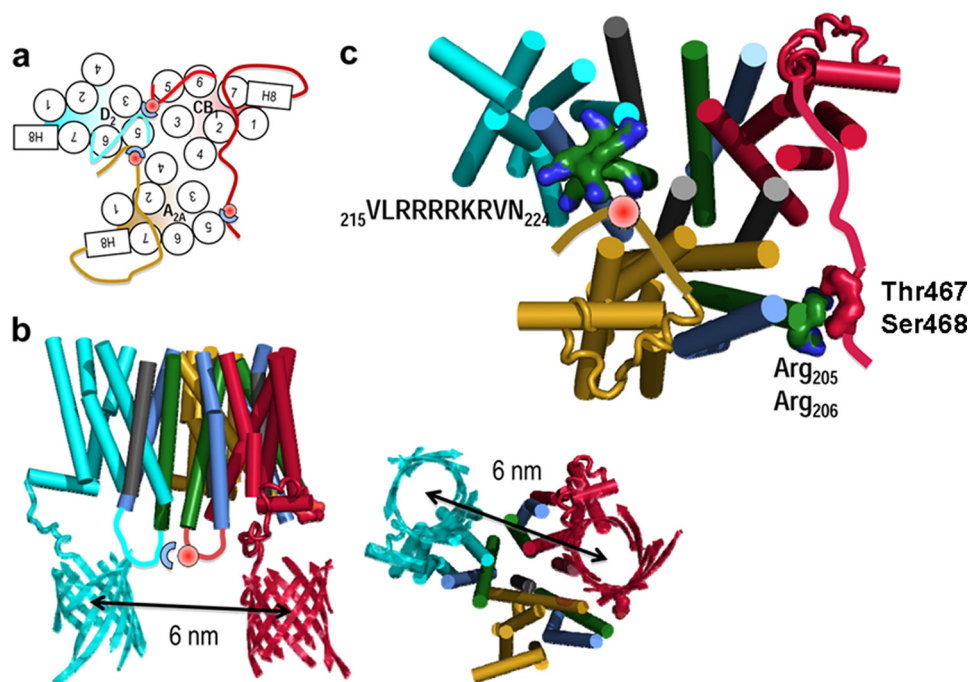


FIGURE 8. Molecular model of the A_{2A} - CB_1 - D_2 receptor heteromer. *a*, schematic model of the heteromerization of A_{2A} (gold), CB_1 (red), and D_2 (cyan) receptors. Solid lines between TM5 and -6 symbolize IL3 of CB_1 (red line, 29 amino acids long) or D_2 (cyan line, 142 amino acids long) receptors, which were not modeled; solid lines after HX8 represent CT of CB_1 (red line) or A_{2A} (gold line), which were arbitrarily modeled as in squid rhodopsin; red spheres represent either phosphorylated Thr³²¹(IL3)-Ser³²²(IL3) or Thr⁴⁶⁷(CT)-Ser⁴⁶⁸(CT) of CB_1 or phosphorylated Ser³⁷⁴(CT) of A_{2A} ; and blue half-circles represent either Arg²⁰⁵(5.66)-Arg²⁰⁶(5.67) of A_{2A} or the ²¹⁵(5.64)VLRRRRKRNVN²²⁴ or ²⁶⁶NRRRVEAARR²⁷⁵(IL3) epitopes of D_2 . *b*, lateral and cytoplasmic views of the computational model of the A_{2A} - CB_1 - D_2 receptor heteromer. GFP fused to Cys⁴⁴³(CT) of the D_2 receptor (cyan surface) and YFP fused to Leu⁴⁷²(CT) of the CB_1 receptor (red surface) are shown. IL3 of CB_1 (red line) and D_2 (cyan line) receptors are shown in solid lines to illustrate their proximity. *c*, cytoplasmic view of the computational model of the A_{2A} - CB_1 - D_2 receptor heteromer. CT of the CB_1 receptor is depicted in the following manner: amino acids Ser⁴¹⁴-Asn⁴³⁷ of (red tube ribbon) are modeled as in the crystal structure of squid rhodopsin, amino acids Asn⁴³⁷-Asp⁴⁶⁶ (not modeled) are shown as a red solid line to illustrate the position of Thr⁴⁶⁷-Ser⁴⁶⁸, and amino acids Ala⁴⁶⁹-Leu⁴⁷² (red solid line) are arbitrarily modeled to position YFP. CT of the A_{2A} receptor is depicted in the following manner: amino acids Ser³⁰⁵-Gly³²⁸ (golden tube ribbon) are modeled as in the crystal structure of squid rhodopsin; amino acids Ser³²⁹-Ser⁴¹² (not modeled) are shown as a yellow solid line, and phosphorylated Ser³⁷⁴ is shown as a red circle. Helices are shown as cylinders with the following color codes: TM4 in gray, TM5 in green, TM6 in blue, and the other helices in yellow for A_{2A} , in red for CB_1 , and cyan for D_2 receptors.

Modeling the A_{2A} - CB_1 - D_2 Receptor Heteromer—The quaternary structure of the A_{2A} - CB_1 - D_2 heteromer was finally obtained by combining the CB_1 - D_2 (TM5-TM5 interface) and CB_1 - A_{2A} (TM4-TM4^{invag}) models described above (Fig. 8*a*). This combination of TM-TM interactions was selected among the others because it best reproduces the distance between GFP and YFP in the proposed A_{2A} - CB_1 - D_2 receptor heteromer within the 5.7–6.1-nm range experimentally determined from FRET efficiencies (see above). Fig. 8*b* shows a molecular model of the A_{2A} - CB_1 - D_2 heteromer, in which GFP was fused to Cys⁴⁴³(CT) of the D_2 receptor at the end of the conserved Hx8; YFP was fused to Leu⁴⁷²(CT) of the CB_1 receptor, only four amino acids apart from the phosphorylated Ser⁴⁶⁸(CT); and Thr⁴⁶⁷(CT)-Ser⁴⁶⁸(CT) of the CB_1 receptor could interact with Arg²⁰⁵(5.66)-Arg²⁰⁶(5.67) of the A_{2A} receptor. In addition, this computational model of the A_{2A} - CB_1 - D_2 receptor heteromer positioned the CT of the A_{2A} receptor toward the D_2 receptor epitope located in the cytoplasm at the end of TM5, so that phosphorylated Ser³⁷⁴(CT) can interact with the (5.64) ²¹⁵VLR-RRRRKRNVN²²⁴ epitope (Fig. 8, *a* and *c*).

As shown above, expression of the CB_1 ^{A467-A468}-YFP or A_{2A} ^{A374}-Rluc mutant receptors leads to a separation of the CT

of CB_1 from A_{2A} and the CT of A_{2A} from D_2 , respectively. This clearly suggests that phosphorylated Thr⁴⁶⁷(CT)-Ser⁴⁶⁸(CT) in CB_1 or Ser³⁷⁴(CT) in A_{2A} serves to maintain the large and flexible CT of the receptors in the proper conformation by interacting with the Arg-rich epitope of the corresponding promoter. It thus seems reasonable to suggest that the absence of Thr⁴⁶⁷(CT)-Ser⁴⁶⁸(CT) in CB_1 or Ser³⁷⁴(CT) in A_{2A} modifies the CT of the mutant receptors, whereas the packing of the TMs in the A_{2A} - CB_1 - D_2 heteromer remains similar.

Structure-Function Relationship in the A_{2A} - CB_1 - D_2 Receptor Heteromer—We explored the possibility that changes in the quaternary structure of A_{2A} - CB_1 - D_2 receptor heteromer after disruption of the electrostatic interactions could correlate with changes in the receptor heteromer function. We first looked for differences in signaling (activation of the MAPK pathway) in cells co-expressing A_{2A} and D_2 receptors in the absence and presence of CB_1 receptors (Fig. 9). In cells co-expressing A_{2A} and D_2 receptors, co-activation of both receptors with their respective selective agonists CGS 21680 (200 nM) and quinpirole (1 μ M) produced a similar degree of ERK1/2 phosphorylation than activation of either A_{2A} or D_2 receptors.

As shown in Fig. 9*a*, the additional co-expression of CB_1 receptor produced a qualitatively different pattern with a significantly higher effect of co-activation of A_{2A} and D_2 receptors compared with cells expressing only A_{2A} and D_2 receptors. We then demonstrated that this pattern of MAPK activation is a biochemical characteristic of the A_{2A} - CB_1 - D_2 receptor heteromer, because it depends on the integrity of its quaternary structure. In fact, we found that it particularly depends on the integrity of the intracellular electrostatic interactions that the CB_1 receptor forms with the D_2 receptor in A_{2A} - CB_1 - D_2 receptor heteromer. Thus, in cells expressing CB_1 ^{A321-A321} or D_2 ^{S25} receptors (which lose the ability to establish electrostatic interactions with the D_2 or the CB_1 receptors, respectively, in the A_{2A} - CB_1 - D_2 receptor heteromer), the pattern of MAPK activation was significantly altered and qualitatively similar to that observed in cells only co-expressing A_{2A} and D_2 receptors (Fig. 9*b*).

The pattern of MAPK activation could then be used as a biochemical fingerprint of the A_{2A} - CB_1 - D_2 receptor heteromer to detect its presence in the brain (3). In fact, comparing the pattern of ERK1/2 phosphorylation upon activation of A_{2A} and D_2 receptors in striatal slices from wild-type mice and CB_1

Quaternary Structure of Receptor Heteromers

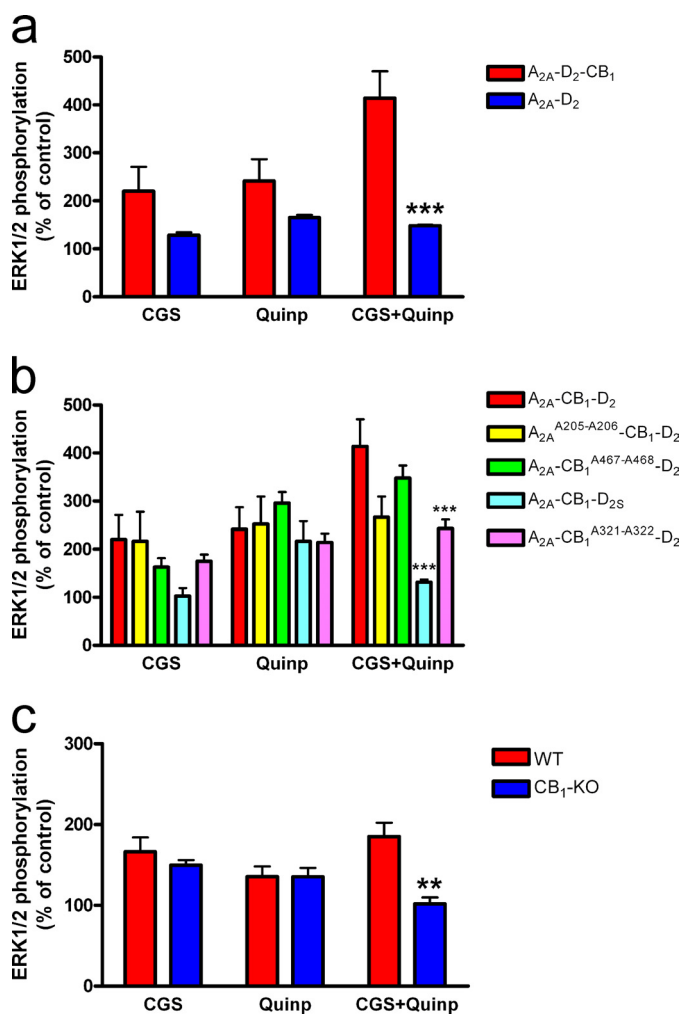


FIGURE 9. Agonist-induced ERK1/2 phosphorylation by the A_{2A}-D₂-CB₁ receptor heteromer. *a* and *b*, assays were performed 48 h post-transfection in cells expressing the indicated receptors (1.2 μ g of cDNA of the A_{2A} or the A_{2A}^{A205-A206} receptors, 1 μ g of cDNA of the D₂, 0.8 μ g of cDNA of the D_{2S} receptor, and 1 μ g of cDNA of the CB₁, CB₁^{A467-A468}, or the CB₁^{A321-A322} receptors). Cells were treated for 5 min with 200 nM CGS 21680 (CGS), 1 μ M quinpirole (Quinip), or both (CGS+Quinip) and ERK1/2 phosphorylation was determined as indicated under "Experimental Procedures." The immunoreactive bands from four experiments performed in duplicate were quantified, and the values represent the mean \pm S.E. of phosphorylation relative to the basal levels found in untreated cells. *c*, assays were performed in striatal slices from wild-type (WT) or CB₁ knock-out mice (CB₁-KO). The slices were treated for 10 min with 1 μ M CGS 21680 (CGS), 1 μ M quinpirole (quinpirole) or both, and ERK1/2 phosphorylation was determined as indicated under "Experimental Procedures." The immunoreactive bands from four to eight slices obtained from five to nine animals were quantified, and values represent the mean \pm S.E. of the % of phosphorylation relative to basal levels found in untreated slices. Significant differences respect to the wild-type mice were calculated by bifactorial ANOVA followed by post hoc Bonferroni's tests (**, $p < 0.01$; ***, $p < 0.001$).

receptor knock-out mice, we found the same qualitative differences as those observed in co-transfected cells with and without CB₁ receptors (compare Fig. 8, *a* and *c*). Thus, in striatal slices from CB₁ receptor knock-out mice, there was a significantly lower ERK1/2 phosphorylation upon co-activation of A_{2A} and D₂ receptors compared with that obtained from striatal slices from wild-type animals. A bifactorial ANOVA demonstrated a significant genotype effect ($p < 0.05$) and significant treatment/genotype interaction ($p < 0.05$), and post hoc Bonferroni tests only showed a significant difference between both groups when

the striatal slices were co-treated with CGS 21680 (1 μ M) and quinpirole (1 μ M) (Fig. 9*c*).

DISCUSSION

This study shows, for the first time, that GPCR heteromers display emerging properties that depend on their folding into a certain quaternary structure, determined not only by interactions between TM domains but also involving interactions between hydrophilic intracellular domains. Significantly, we have found that each receptor, A_{2A}, CB₁, and D₂, contains two key intracellular domains to interact in a selective manner with intracellular domains of the other two receptors by means of electrostatic interactions in the formation of the quaternary structure of the A_{2A}-D₂, A_{2A}-CB₁, CB₁-D₂, and A₁-CB₁-D₂ receptor heteromers. Thus, the D₂ receptor contains two Arg-rich epitopes, ²¹⁵VLRRRR-KRVN²²⁴ and ²⁶⁶NRRRVEAARR²⁷⁵, that interact with potential CK1/2-dependent phosphorylatable Ser/Thr residues in CT (Ser³⁷⁴) of the A_{2A} receptor and in IL3 (Thr³²¹-Ser³²²) of the CB₁ receptor, respectively; CB₁ receptor contains adjacent phosphorylatable Ser and Thr residues in IL3 (Thr³²¹ and Ser³²²) and the CT (Thr⁴⁶⁷ and Ser⁴⁶⁸) that interact with Arg residues in IL3 (²⁶⁶NRRRVEAARR²⁷⁵) of the D₂ receptor and Arg²⁰⁵-Arg²⁰⁶ of the A_{2A} receptor, respectively; and the A_{2A} receptor contains Arg residues at the end of TM5 in the cytoplasm at Arg²⁰⁵-Arg²⁰⁶ and a phosphorylatable Ser residue in the CT (Ser³⁷⁴), which interact with phosphorylatable Ser/Thr residues in the CB₁ receptor CT (Thr⁴⁶⁷ and Ser⁴⁶⁸) and an Arg-rich epitope of the D₂ receptor located in the cytoplasm at the end of TM5 (²¹⁵VLRRRR-KRVN²²⁴), respectively. The fact that each of these three receptors forms electrostatic interactions involving evolutionarily conserved adjacent Arg residues and CK1/2-dependent phosphorylatable Ser and Thr residues with the other two receptors suggests that these particular electrostatic interactions constitute a general mechanism for receptor heteromerization. In studies using synthetic peptides, it has been shown that these electrostatic interactions are particularly stable. Thus, the Arg-phosphate interaction is so stable that when using collision-induced dissociation, the noncovalent interactions between the Arg guanidinium groups and the phosphate group remain intact even though the covalent bond between the serine and phosphate breaks (16, 31–33).

Using bioluminescence resonance energy transfer techniques with mutant receptors, we propose for the first time the quaternary structure for three interacting GPCRs. Characterization of protomer organization within the A₁-CB₁-D₂ receptor heteromer requires, in addition to our findings, integration of information from a variety of different approaches. Most compelling are studies that apply disulfide cross-linking to map TM interfaces between protomers (10, 12, 13). Modeling of the CB₁-D₂, A_{2A}-CB₁, and A_{2A}-D₂ receptor heterodimers was performed through the entire set of proposed TM interfaces (*i.e.* TM1, TM4, or TM5). Our results are compatible with models proposed for other family A GPCRs, where oligomerization involves primarily TM4 and TM5 interfaces (Fig. 8). Thus, our study supports a triangular rather than a linear arrangement of receptors in the A_{2A}-CB₁-D₂ heteromer. This arrangement allows the possibility of simultaneous homodimerization of

each receptor unit using the TM1 interface, which is a well established phenomenon in the GPCR field. Thus, this study opens up a new conceptual challenge in the field of receptor heteromerization, which is the idea that GPCRs can form not only heteromultimers of three different receptor units but also higher order heteromultimers or “receptor nets.”

The interactions of the intracellular domains of the CB₁ receptor with A_{2A} and D₂ receptors were found to be fundamental for the correct formation of the quaternary structure needed for the function of the A_{2A}-CB₁-D₂ receptor heteromers. Thus, mutant receptors lacking the interacting amino acids significantly disrupted RET and a specific qualitative pattern of ERK1/2 phosphorylation induced by co-activation of A_{2A} and D₂ receptors. The fact that such a disruption of the quaternary structure of the A_{2A}-CB₁-D₂ receptor heteromer (as demonstrated by SRET experiments) was associated with a significant qualitative change in signaling indicates that electrostatic interactions between intracellular domains are also key determinants for the specific biochemical properties of the A_{2A}-CB₁-D₂ receptor heteromer. These biochemical characteristics and the specific qualitative pattern of MAPK activation could be used as a biochemical fingerprint of the A_{2A}-CB₁-D₂ receptor heteromer presence in the brain. CB₁ receptor KO mice experiments provided strong support for the existence of A_{2A}-CB₁-D₂ receptor heteromer in the striatum. It has been hypothesized that A_{2A}-CB₁-D₂ receptor heteromers are mostly located in one subtype of striatal neuron, the GABAergic enkephalinergic neuron, where the three receptors are highly co-expressed and exert a significant control of basal ganglia function (34). Most probably, the results obtained with MAPK signaling are just a minor but the first described example of many of the potential properties of the A_{2A}-CB₁-D₂ receptor heteromers.

Acknowledgments—We thank Prof. Olga Valverde and Prof. Catherine Ledent (Department of Experimental and Health Sciences, Biomedical Research Park, Barcelona University Pompeu Fabra, Barcelona, Spain) for generously supplying wild-type and CB₁ receptor KO mice. We thank the Office of National Drug Control Policy and Jodie Franklin (The Johns Hopkins Synthesis and Sequencing Facility) for the peptide synthesis. We acknowledge the technical help obtained from Jasmina Jiménez (Molecular Neurobiology Laboratory, Barcelona University).

REFERENCES

- Ferré, S., Ciruela, F., Woods, A. S., Lluís, C., and Franco, R. (2007) *Trends Neurosci.* **30**, 440–446
- Pin, J. P., Neubig, R., Bouvier, M., Devi, L., Filizola, M., Javitch, J. A., Lohse, M. J., Milligan, G., Palczewski, K., Parmentier, M., and Spedding, M. (2007) *Pharmacol. Rev.* **59**, 5–13
- Ferré, S., Baler, R., Bouvier, M., Caron, M. G., Devi, L. A., Durrour, T., Fuxe, K., George, S. R., Javitch, J. A., Lohse, M. J., Mackie, K., Milligan, G., Pflieger, K. D., Pin, J. P., Volkow, N. D., Waldhoer, M., Woods, A. S., and Franco, R. (2009) *Nat. Chem. Biol.* **5**, 131–134
- Dalrymple, M. B., Pflieger, K. D., and Eidne, K. A. (2008) *Pharmacol. Ther.* **118**, 359–371
- Carriba, P., Navarro, G., Ciruela, F., Ferré, S., Casadó, V., Agnati, L., Cortés, A., Mallol, J., Fuxe, K., Canela, E. I., Lluís, C., and Franco, R. (2008)

- Nat. Methods* **5**, 727–733
- Gandia, J., Galino, J., Amaral, O. B., Soriano, A., Lluís, C., Franco, R., and Ciruela, F. (2008) *FEBS Lett.* **582**, 2979–2984
- Davies, A., Gowen, B. E., Krebs, A. M., Schertler, G. F., and Saibil, H. R. (2001) *J. Mol. Biol.* **314**, 455–463
- Maurel, D., Comps-Agrar, L., Brock, C., Rives, M. L., Bourrier, E., Ayoub, M. A., Bazin, H., Tinel, N., Durrour, T., Prézéau, L., Trinquet, E., and Pin, J. P. (2008) *Nat. Methods* **5**, 561–567
- Fotiadis, D., Liang, Y., Filipek, S., Saperstein, D. A., Engel, A., and Palczewski, K. (2003) *Nature* **421**, 127–128
- Klco, J. M., Lassere, T. B., and Baranski, T. J. (2003) *J. Biol. Chem.* **278**, 35345–35353
- Liang, Y., Fotiadis, D., Filipek, S., Saperstein, D. A., Palczewski, K., and Engel, A. (2003) *J. Biol. Chem.* **278**, 21655–21662
- Guo, W., Shi, L., Filizola, M., Weinstein, H., and Javitch, J. A. (2005) *Proc. Natl. Acad. Sci. U.S.A.* **102**, 17495–17500
- Guo, W., Urizar, E., Kralikova, M., Mobarec, J. C., Shi, L., Filizola, M., and Javitch, J. A. (2008) *EMBO J.* **27**, 2293–2304
- González-Maeso, J., Ang, R. L., Yuen, T., Chan, P., Weisstaub, N. V., López-Giménez, J. F., Zhou, M., Okawa, Y., Callado, L. F., Milligan, G., Gingrich, J. A., Filizola, M., Meana, J. J., and Sealton, S. C. (2008) *Nature* **452**, 93–97
- Han, Y., Moreira, I. S., Urizar, E., Weinstein, H., and Javitch, J. A. (2009) *Nat. Chem. Biol.* **5**, 688–695
- Woods, A. S., and Ferré, S. (2005) *J. Proteome Res.* **4**, 1397–1402
- Zimmermann, T., Rietdorf, J., Girod, A., Georget, V., and Pepperkok, R. (2002) *FEBS Lett.* **531**, 245–249
- Ledent, C., Valverde, O., Cossu, G., Petitet, F., Aubert, J. F., Beslot, F., Böhme, G. A., Imperato, A., Pedrazzini, T., Roques, B. P., Vassart, G., Fratta, W., and Parmentier, M. (1999) *Science* **283**, 401–404
- Aso, E., Ozaita, A., Valdizán, E. M., Ledent, C., Pazos, A., Maldonado, R., and Valverde, O. (2008) *J. Neurochem.* **105**, 565–572
- Jaakola, V. P., Griffith, M. T., Hanson, M. A., Cherezov, V., Chien, E. Y., Lane, J. R., Ijzerman, A. P., and Stevens, R. C. (2008) *Science* **322**, 1211–1217
- Cherezov, V., Rosenbaum, D. M., Hanson, M. A., Rasmussen, S. G., Thian, F. S., Kobilka, T. S., Choi, H. J., Kuhn, P., Weis, W. I., Kobilka, B. K., and Stevens, R. C. (2007) *Science* **318**, 1258–1265
- Rasmussen, S. G., Choi, H. J., Rosenbaum, D. M., Kobilka, T. S., Thian, F. S., Edwards, P. C., Burghammer, M., Ratnala, V. R., Sanishvili, R., Fischetti, R. F., Schertler, G. F., Weis, W. I., and Kobilka, B. K. (2007) *Nature* **450**, 383–387
- Ballesteros, J. A., and Weinstein, H. (1995) in *Methods in Neurosciences*, Vol. 25, pp. 366–428, Elsevier, San Diego, CA
- Park, J. H., Scheerer, P., Hofmann, K. P., Choe, H. W., and Ernst, O. P. (2008) *Nature* **454**, 183–187
- Murakami, M., and Kouyama, T. (2008) *Nature* **453**, 363–367
- Li, J., Edwards, P. C., Burghammer, M., Villa, C., and Schertler, G. F. (2004) *J. Mol. Biol.* **343**, 1409–1438
- Blom, N., Gammeltoft, S., and Brunak, S. (1999) *J. Mol. Biol.* **294**, 1351–1362
- Ciruela, F., Burgueño, J., Casadó, V., Canals, M., Marcellino, D., Goldberg, S. R., Bader, M., Fuxe, K., Agnati, L. F., Lluís, C., Franco, R., Ferré, S., and Woods, A. S. (2004) *Anal. Chem.* **76**, 5354–5363
- Azdad, K., Gall, D., Woods, A. S., Ledent, C., Ferré, S., and Schiffmann, S. N. (2009) *Neuropsychopharmacology* **34**, 972–986
- Missale, C., Nash, S. R., Robinson, S. W., Jaber, M., and Caron, M. G. (1998) *Physiol. Rev.* **78**, 189–225
- Jackson, S. N., Wang, H. Y., and Woods, A. S. (2005) *J. Proteome Res.* **4**, 2360–2363
- Jackson, S. N., Moyer, S. C., and Woods, A. S. (2008) *J. Am. Soc. Mass Spectrom.* **19**, 1535–1541
- Jackson, S. N., Wang, H. Y., Yergey, A., and Woods, A. S. (2006) *J. Proteome Res.* **5**, 122–126
- Ferré, S., Goldberg, S. R., Lluís, C., and Franco, R. (2009) *Neuropharmacology* **56**, Suppl. 1, 226–234

Interactions between Intracellular Domains as Key Determinants of the Quaternary Structure and Function of Receptor Heteromers

Gemma Navarro, Sergi Ferré, Arnau Cordomi, Estefania Moreno, Josefa Mallol, Vicent Casadó, Antoni Cortés, Hanne Hoffmann, Jordi Ortiz, Enric I. Canela, Carme Lluís, Leonardo Pardo, Rafael Franco and Amina S. Woods

J. Biol. Chem. 2010, 285:27346-27359.

doi: 10.1074/jbc.M110.115634 originally published online June 18, 2010

Access the most updated version of this article at doi: [10.1074/jbc.M110.115634](https://doi.org/10.1074/jbc.M110.115634)

Alerts:

- [When this article is cited](#)
- [When a correction for this article is posted](#)

[Click here](#) to choose from all of JBC's e-mail alerts

Supplemental material:

<http://www.jbc.org/content/suppl/2010/06/18/M110.115634.DC1>

This article cites 34 references, 7 of which can be accessed free at <http://www.jbc.org/content/285/35/27346.full.html#ref-list-1>